MODELING, DESIGN, AND CONTROL OF FORCED-FEEDBACK METERING POPPET VALVE SYSTEM

A Thesis presented to the faculty of the Graduate School
University of Missouri-Columbia

In Partial Fulfillment
Of the Requirements for the Degree
Master of Science

---

by

MATTHEW MULLER

Dr. Roger Fales, Thesis Supervisor

May 2006

The undersigned, appointed by the dean of the Graduate School, have examined the project entitled

MODELING, DESIGN, AND CONTROL OF FORCED-FEEDBACK METERING POPPET VALVE SYSTEM

Presented by MATTHEW MULLER

a candidate for the degree of Masters of Science

and hereby certify that in their opinion it is worthy of acceptance

---

Dr. Roger C. Fales, Assistant Professor, Mechanical and Aerospace Engineering

---

Dr. Noah Manring, J.C. Dowell Prof (MAE), Associate Dean of Research (CoE)

Dr. Steven C. Borgelt, Associate Professor, Biological Engineering

ACKNOWLEDGMENTS

The opportunity to attend graduate school at the University of Missouri has been a blessing that I have found continually challenging and rewarding. I am forever grateful to all the teachers and friends whom have constantly dealt with my endless questions.

I am especially thankful to my academic advisor, Dr. Roger Fales for his constant patience and willingness to teach me the many aspects of hydraulics and controls theory. If it were not for his support, I would not know what a metering poppet valve was, let alone be able to deal with the many obstacles this research presented.

I am also thankful to Dr. Manring for his open door to my questions regarding hydraulics and his accepting to serve on my thesis committee. His knowledge and his book have provided a constant resource for this project.

I express my appreciation to Dr. Borgelt for generously giving up his time to examine my thesis and serve on my masters committee.

I will forever be grateful to my parents whom have always encouraged the quest for knowledge and whose example provides endless motivation.

Last and most profoundly, I owe this entire experience to my wife JoAnn who not only listened to my daily challenges but made it possible for me to return to graduate school.

TABLE OF CONTENTS

Acknowledgements……ii

List of Figures……..…vi

Abstract……..xi

Chapter 1. Introduction……1

1.1 Motivation and Literature Review……...1

1.2 Research Objectives……2

1.3 Forced Feedback Principles……3

1.4 Thesis Outline……6

Chapter 2. Mathematical Modeling of the Constant Orifice Approach……8

2.1 Nonlinear Constant Orifice Model……8

2.2 Model Linearization……10

Chapter 3. Iterative Root Locus Analysis and Design……13

3.1 Iterative Design Procedure……13

3.2 Root Locus Plots for the Constant Orifice Model……14

Chapter 4. Variable Orifice Vs. Constant Orifice Models……22

4.1 Equations for the Variable Orifice Model……22

4.2 Criteria for Constant Verses Variable Orifice Model Comparisons…..22

4.3 Simulation Comparisons……25

4.4 Design Information Obtained from Model Comparisons……28

Chapter 5. Examination of Previously Unmodeled Dynamics……32

5.1 An 8-State Model……32

5.2 Validation of 8-State Model Linearization……34

5.3 8-State vs. 5-State Model……37

Chapter 6. Mechanical and Electronic Control Designs……41

6.1 Introduction to Flow Control……..……41

6.2 Mechanical Pressure Compensation for Flow Control……42

6.3 Electronic Flow Control……...44

6.3.1 Table Look-up Control……44

6.3.2 Table Look-up with PD Control……48

6.3.3 Gain Scheduled PD Control……..51

6.3.4 Table Look-up with Gain Scheduled PD Control……...54

6.4 Flow Control Summary……56

6.5 Observer Design……..57

Chapter 7. Robust Control Analysis……64

7.1 Introduction to Robust Analysis……64

7.2 Nominal Performance and the Sensitivity Transfer Function……..65

7.3 Derivation of Robust Stability with Multiplicative Uncertainty……...67

7.4 Multiplicative Uncertainty Weighting Function W_I……...69

7.5 Robust Stability and Performance Results……..71

Chapter 8. Conclusions……..73

8.1 Overview……73

8.2 Research limitations……75

8.3 Scope for future work……..75

Appendix…………………………………………………………………………..…77

References…………………………………………………………………………..…80

LIST OF FIGURES

Fig. 1.1 Forced feedback poppet configuration 4

Fig. 1.2 Forced feedback poppet with a constant inlet orifice to control volume ... 6

Fig. 3.1 Root locus varying a_1 $(P_s = 21MPa, \Delta P \approx 2.1MPa)$ $f = 5N$ 15

Fig. 3.2 Zoom of the right portion of Fig. 3.1 15

Fig. 3.3 Root locus varying h_3 $(P_s = 21MPa, \Delta P \approx 2.1MPa)$ $f = 5N$ 16

Fig. 3.4 Root locus varying h_2 $(P_s = 21MPa, \Delta P \approx 2.1MPa)$ $f = 5N$ 16

Fig. 3.5 Root locus varying k (spring rate) $(P_s = 21MPa, \Delta P \approx 2.1MPa)$ $f = 5N$ 17

Fig. 3.6 Root locus varying b_x (pilot damping) $(P_s = 21MPa, \Delta P \approx 2.1MPa)$ $f = 5N$ 17

Fig. 3.7 Root locus varying k $(P_s = 21MPa, \Delta P \approx 2.1MPa)$ $f = 30N$ 19

Fig. 3.8 Root locus varying a_1 $(P_s = 35MPa \ \ \Delta P \approx 35MPa)$ $f = 5N$ 19

Fig. 3.9 Root locus varying k $(P_s = 35MPa \ \ \Delta P \approx 35MPa)$ $f = 5N$ 20

Fig. 3.10 Root locus varying kc_4 $(P_s = 21MPa, \Delta P \approx 2.1MPa)$ $f = 5N$ 20

Fig. 4.1 Control volume inlet and outlet orifices 23

Fig. 4.2 Roots for linearization with 2.1 MPa pressure drop and valve open 0.2 mm 24

Fig. 4.3 Zoom in for the roots on the right side of Fig. 4.2 24

Fig. 4.4 Frequency response for both models $(P_s = 21MPa, \Delta P = 1MPa)$ 25

Fig. 4.5 Main poppet position in response to step input force from 0-.2 s, F=50.2

N for variable orifice, F= 51.4 for constant orifice $(P_s = 2.1MPa, \Delta P = 1MPa)$ 26

Fig. 4.6 Main poppet position in response to step input force, F=48.8 N for variable orifice, F= 54.6 for constant orifice $(P_s = 35MPa, \Delta P \approx 35MPa)$ 26

Fig. 4.7 Flow out of the control volume for main poppet response of Fig. 4.6 $(P_s = 35MPa, \Delta P \approx 35MPa)$ 27

Fig. 4.8 Main poppet cracked open in response to step input force, F=8.1 N for variable orifice, F=13.6 N for constant orifice $(P_s = 35MPa, \Delta P \approx 35MPa)$ 28

Fig. 4.9 Main poppet response to a solenoid input force from 0-.2 s. Constant orifice model modified for stability as compared to Fig. 4.5 $(P_s = 2.1MPa, \Delta P = 1MPa)$ 29

Fig. 4.10 Main poppet response to solenoid input force. Constant orifice model modified for stability as compared to Fig. 4.6 $(P_s = 35MPa, \Delta P \approx 35MPa)$ 30

Fig. 4.11 Frequency response for both versions of the constant orifice model $(P_s = 21MPa, \Delta P = 1MPa)$ 31

Fig. 5.1 Main poppet position for a unit step input 35

Fig. 5.2 Main poppet velocity for a unit step input..... 35

Fig. 5.3 Pilot poppet position for a unit step input 35

Fig. 5.4 Pilot poppet velocity for a unit step input 36

Fig. 5.5 Control volume pressure for a unit step input 36

Fig. 5.6 Pilot control volume pressure for a unit step input 36

Fig. 5.7 Load volume pressure for a unit step input..... 37

Fig. 5.8 Load piston velocity for a unit step input 37

Fig. 5.9 Roots for linearization with valve open 0.2 mm ($P_s = 21MPa, \Delta P \approx 2.1MPa$) . 38

Fig. 5.10 Zoom in for the right side of Fig. 5.9 38

Fig. 5.11 Frequency response for both versions of the constant orifice model ($P_s = 21MPa, \Delta P = 1MPa$) 40

Fig. 6.1 System with compensator, metering poppet valve, and load 42

Fig. 6.2 Valve flow for pressure compensated models (desired flow 30LPM) ... 43

Fig. 6.3 Pressure drop from supply to load pressure 43

Fig. 6.4 Poppet valve control scheme with look-up table 44

Fig. 6.5 Look-up table control vs pressure compensation, desired flow 30 LPM, see Fig. 6.3 for pressure drop 45

Fig. 6.6 Look-up table control vs pressure compensation, desired flow 110 LPM, see Fig. 6.3 for pressure drop 46

Fig. 6.7 Varying desired flow between 10 and 100 LPM, pressure drop approx 30MPa 47

Fig. 6.8 Varying desired flow between 10 and 70 LPM, pressure drop approx 1 MPa 47

Fig. 6.9 Electronic control with look-up table and PD control 48

Fig. 6.10 Look-up table control vs look-up plus PD control, desired flow 110 LPM, see Fig. 6.3 for pressure drop 49

Fig. 6.11 Varying desired flow between 10 and 100 LPM, pressure drop approx

30MPa 50
Fig. 6.12 Varying desired flow between 10 and 70 LPM, pressure drop approx 1 MPa 50
Fig. 6.13 Root locus for negative feedback of flow (35 Mpa pressure drop) 52
Fig. 6.14 Root locus for negative feedback of flow (1 Mpa pressure drop) 52
Fig. 6.15 Gained scheduled PD controller based on measured pressure drop .. 53
Fig. 6.16 Look-up table control vs gain scheduled PD control, desired flow 110 LPM, see Fig. 6.3 for pressure drop 53
Fig. 6.17 Varying desired flow between 10 and 100 LPM, pressure drop approx 30 MPa 54
Fig. 6.18 Varying desired flow between 10 and 70 LPM, pressure drop approx 1 MPa 54
Fig. 6.19 Gain scheduled Pd control with look-up table 55
Fig. 6.20 Look-up table control vs look-up table with gained PD control, desired flow 110 LPM, see Fig. 6.3 for pressure drop 55
Fig. 6.21 Varying desired flow between 10 and 100 LPM, pressure drop approx 30MPa 56
Fig. 6.22 Varying desired flow between 10 and 70 LPM, pressure drop approx 1 MPa 56
Fig. 6.23 Observer estimate of main poppet position 59
Fig. 6.24 Observer estimate of main poppet velocity 60
Fig. 6.25 Observer estimate of pilot poppet position 60

Fig. 6.26 Observer estimate of pilot poppet velocity 60

Fig. 6.27 Observer estimate of pressure above main poppet 61

Fig. 6.28 Observer estimate of pressure above pilot poppet 61

Fig. 6.29 Observer estimate of load pressure (measured) 61

Fig. 6.30 Observer estimate of load piston velocity 62

Fig. 6.31 Observer flow estimate vs. 'true' flow 63

Fig. 7.1 PD/table look-up control with pressure drop held constant 66

Fig. 7.2 Block diagram reduction for calculating sensitivity transfer function 66

Fig. 7.3 Nominal Performance for 3 pressure drops when the valve is cracked open 67

Fig. 7.4 Control scheme with multiplicative uncertainty included 68

Fig. 7.5 $N\Delta$ configuration for determining RS criteria 68

Fig. 7.6 Block diagram for determining robust stability criterion 69

Fig. 7.7 W_I for worst case plant at 1 MPa pressure drop 71

Fig. 7.8 Robust stability for 3 pressure drops with the valve cracked open 72

Fig. 7.9 Robust performance for 3 pressure drops with the valve cracked open 72

ABSTRACT

This research explores valve design, dynamic modeling, and techniques to achieve flow control for a forced-feedback metering poppet valve system. In particular, nonlinear and linear models of a forced feedback configuration are developed and tuned through the use of root locus techniques. Typical steady state conditions as well as extreme high and low pressure drops are simulated in attempts to uncover instabilities and other possible undesirable performance characteristics of the valve. It is shown that by using a variable inlet orifice to the control volume as opposed to a constant orifice, desired system bandwidth and stability can be achieved. Open loop valve designs are then simulated with several electronic control schemes which incorporate feedback of load pressure and in some cases valve flow. An observer design is investigated as a means of providing flow feedback without additional sensor costs. Electronic flow control schemes are compared to standard mechanical pressure compensation and finally a robust analysis is provided for a chosen electronic control scheme.

CHAPTER 1

INTRODUCTION

1.1 Motivation and Literature Review:

Electro-hydraulic control valves are extensively used in industry to control motion in various devices. For many years the standard has been to use spool type valves along with separate supply pressures for the pilot and main stages of flow control valves. Poppet valves have been available for many years but have been limited in use to situations such as pressure relief. Over the past ten years there has been a push to develop poppet valves that can meter flow in the way spool valves have typically been used [1,2,3,4,5]. The incentives behind this growing trend are the advantages that come with the use of poppet valves. In comparison to spool valves, poppet valves require less stringent machining tolerances, are less susceptible to contamination problems, have very low leakage, and make it possible to eliminate two separate supply lines [6,7]. Although poppet valves present many advantages to spool valves they have yet to take over the market due to a long history of instability issues. The instabilities in poppet valve circuits have been studied by Hayashi [8] , Funk [9], Wandling [10], and others but there is still no clear path to avoiding this problem. Hayashi

[8] suggests it is important to examine valve motions with small valve lift and hysteresis of flow forces. Funk [9] presents claims that instability can be caused by interaction between the poppet spring-mass system and line dynamics. McCloy [11] examines the effects steady-state flow forces in various valve systems while more recently Johnston et al. [12] provides experimental investigations into poppet flow forces. In recent years there have been metering poppet valves that have proved successful enough to become commercially available. Zhang et al. [1] studies the dynamics of one such valve and suggest performance limitations due to zero location. Fales [13] studies the performance and stability of the same valve as Zang [1] and demonstrates the importance of pressure drop in the analysis. Opdenbosch et al. [14] models a newer poppet valve with a position follower configuration and proposes a controller based on a Nodal Link Perceptron Network. The list of papers in the open literature in regards to modeling the dynamics of metering poppet valves surrounds the few commercially produced valves but there is little to no focus in the literature providing guiding techniques for designing a metering poppet valve from a ground up approach. Although the literature is scarce in regards to the design of metering poppet valves, existing research provides design methods which can be applied to poppet valves. One such example comes from Li [15], who uses root locus analysis to redesign a two-spool flow control servo valve.

1.2 Research Objectives:

The ultimate goal of this research project is to provide methods for

designing a metering poppet valve which is stable while meeting performance requirements. Specifically, it is desired that the poppet valve can accurately meter flow from 0-120 LPM while maintaining a bandwidth of 8 Hertz or greater, where bandwidth is defined as a 3dB drop from the low frequency gain or 0.707 of the low frequency gain in absolute terms. In attempts to achieve the ultimate goal, the following underlying objectives will be the focus of this thesis:

1. Establish a linear and nonlinear mathematical model for a forced feedback metering poppet valve system.
2. Use linear root locus techniques, nonlinear simulations, and Bode plots created from the nonlinear simulations as tools for designing the open-loop valve system.
3. Examine mechanical and electronic methods for providing flow control.
4. Analyze the robustness of electronic control design.

1.3 Forced Feedback Principles:

Fig. 1.1 embodies the forced-feedback electro-hydraulic poppet valve which is the focus of this research. The following is a brief explanation of the workings of the forced feedback poppet portrayed in Fig. 1.1. As shown, the valve is in the closed position with high pressure fluid (supply) connected to the inlet port {13} while low pressure (load) is connected to the outlet port {11}. The main passageway from high to low pressure is sealed by the main poppet {19}, while a passageway {18} connects the control volume {8} to high pressure fluid. High pressure in the control volume {8} holds the main poppet {19} closed via

pressure on its upper surface. The control volume {8} is sealed from the low pressure port {11} via several mechanisms. These are the pilot poppet seat {5}, a ball check on passage {10}, and two dynamic o-ring seals (not shown), which would be found between the main poppet {19} and its land and the pilot poppet {3} and its land.

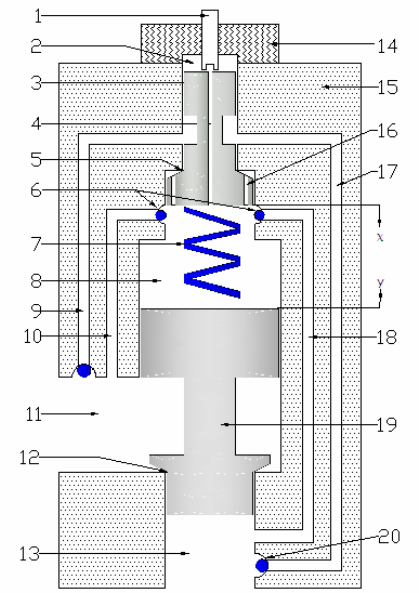

Fig. 1.1 Forced feedback poppet configuration

The pilot poppet {3} is assumed to be pressure balanced via the pilot tube {4} while the feedback spring {7} maintains the pilot poppet {3} in its closed position. In order to raise the main poppet {19} off its seat and control flow, the pilot poppet {3} is opened by a push from the actuator {1}. As the pilot poppet {3} opens, the control volume outlet orifice {5} becomes large enough to create a net outflow of fluid. This net outflow of fluid causes the control volume pressure {8} to decrease to the point that the main poppet {19} begins to lift off its seat. The

main poppet {19} pushes against the feedback spring {7} which in turn pushes pilot poppet {3} back towards its seat. After a short time, an equilibrium position will be reached where both the main poppet {19} and the pilot poppet {3} are open. The final position of the main poppet {19} will depend on the force imparted by the actuator {1}. In order to close the main poppet {19}, the actuator force is turned off allowing the feedback spring {7} to push the pilot poppet {3} back to its seat. The control volume outlet orifice {5} is now closed while high pressure fluid from the inlet passage {18} fills the control volume {8} and pushes the main poppet {19} closed. In the event that load pressure {11} exceeds supply pressure {13}, passage {10} serves as the inlet to the control volume while passage {17} serves as the outlet. Although passages {9}, {10}, {17}, {18}, and their corresponding ball checks make it possible for the valve to provide bidirectional flow this aspect of the valve will not be considered in this research.

Ultimately, the valve design must provide the ability to rapidly move the main poppet {19} to a desired position so as to control flow. Achieving desired performance for the main poppet {19} hinges on being able to quickly reduce or increase the pressure in the control volume {8}. Past forced-feedback configurations have been designed with a fixed inlet orifice {21} to the control volume as shown in Fig. 1.2. Although the design in Fig. 1.2 should be functional, it is thought that a fixed inlet orifice could be a key factor in limiting the performance of this type of valve. One premise of this research is to examine if performance can be improved via the inclusion of a variable inlet orifice {6} to the

control volume as pictured in Fig. 1.1. In reference to Fig. 1.1, opening the pilot poppet {3} both reduces the size of the inlet orifice {6} and opens of the outlet orifice {5}.

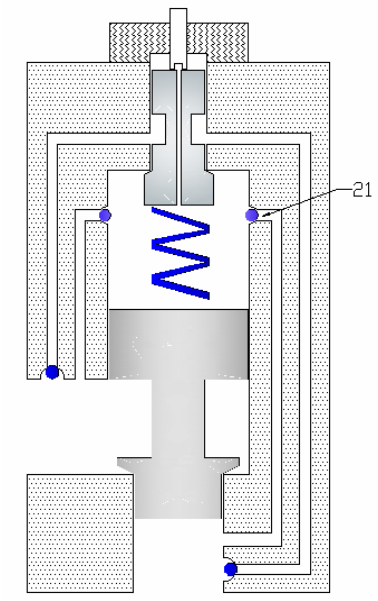

Fig. 1.2 Forced feedback poppet with a constant inlet orifice to control volume

It is hypothesized that this relationship will provide increased pressure rise and fall rates for the control volume {8} and in turn reduce the time it takes to open or close the main poppet {19}. In order to reach meaningful conclusions, both a “constant orifice” (CO) and “variable orifice” (VO) models will be designed and compared.

1.4 Thesis Outline:

In Chapter 2, a mathematical model is developed for the constant orifice model coupled with an external orifice restricting load flow. Basic assumptions are discussed and linearizations are provided. Chapter 3 establishes an iterative

procedure which makes use of linear root locus techniques and nonlinear simulations to enhance the valve design. Root locus plots are presented for the constant orifice model at various operating conditions and useful information is gained regarding how design parameters affect stability and performance. Chapter 4 modifies the constant orifice model to create a variable orifice and then presents side by side design results for the two models when load pressure is held constant. Chapter 5 expands the model presented in Chapter 2 in order to validate assumptions made regarding the pilot poppet damping and the effects of the restricting load orifice. The final 8-state linearized model is then compared with nonlinear simulation results. Chapter 6 explores both electronic and mechanical control while including an initial investigation of observer design. Chapter 7 provides a robust analysis of a particular controller presented and Chapter 6. Finally, Chapter 8 provides conclusions, design limitations, and the scope for future work, while nomenclature can be found in the appendix.

CHAPTER 2

MATHEMATICAL MODELING OF THE CONSTANT ORIFICE APPROACH

2.1 Nonlinear Constant Orifice Model:

Initial equations were derived to reflect the dynamics of the constant orifice model embodied in Fig. 1.2, while geometry was chosen in attempts to produce a flow of 120 LPM with the main poppet fully open and a pressure drop of 2.1 MPa. The general model can be broken into four basic systems or governing equations: two spring mass damper systems with flow and pressure forces for each poppet, a pressure rise rate equation for the control volume, and a pressure rise rate equation for the load volume. The forces acting on the main poppet are represented by Eq. (2-1).

$$M\ddot{y} = -b_y\dot{y} - k(y + x + preload) - P_C A_C + P_s A_s + P_L A_L - 0.72C_d{}^2 h_3 y(P_s - P_L) \quad (2\text{-}1)$$

It is noted that the last term in Eq. (2-1) represents the flow forces on the poppet and that in general flow forces in this paper will be considered to act in a direction such as to restrict the given orifice. It is also noted that the numerical coefficient on the flow force term is the equivalent of two times the cosine of the jet angle, where 69 degrees is a common estimation for this parameter [6]. The forces acting on the pilot poppet are represented by Eq. (2-2), with 'F' representing the

input force from the actuator.

$$m\ddot{x} = -B_x\dot{x} - k(y + x + preload) - 0.72C_d{}^2 h_2 x(P_C - P_L) + F \tag{2-2}$$

Equation (2-2) does not contain the pressure forces which act on each end of the pilot poppet. For simplicity, initial efforts assume the pilot poppet is pressure balanced while accounting for nonlinear damping forces by introducing an artificial linear damping coefficient, B_x, which represents the sum of linear and nonlinear damping. It is noted that later efforts will introduce a more realistic model of the forces acting on the pilot poppet. The change in control volume pressure is given by Eq. (2-3). The assumption has been made that pilot poppet movement has a negligible effect on the pressure of the control volume. This is generally true due to the relatively small area and displacement of the pilot poppet.

$$\dot{P}_C = \frac{\beta}{V_C - A_C y}(Q_1 - Q_2 + A_C\dot{y}) \tag{2-3}$$

Realistically, load pressure is the pressure of the fluid contained between the valve and a working piston cylinder assembly. Although later models incorporate these dynamics, initial design is accomplished by replacing the piston cylinder model with flow across a fixed orifice. The resulting model is shown in Eq. (2-4)

$$\dot{P}_L = \frac{\beta}{V_L}(Q_2 + Q_3 - Q_4) \tag{2-4}$$

In order to simulate a particular pressure drops across the valve, the area of the load orifice can be set as needed. The terms, Q_1 through Q_4, represent classic

orifice flow and are given be Eq. (2-5).

$$Q = aC_d\sqrt{\tfrac{2}{\rho}\Delta P} \tag{2-5}$$

In cases where an orifice is variable, its area varies linearly with poppet position with '*h*' being the slope of the line.

2.2 Model Linearization:

Equations (2-1) through Eq. (2-5) represent a nonlinear model of the forced feedback poppet as shown in Fig. 1.2. Although the nonlinear model is more appropriate for examining valve behavior, a linear simplification and accompanying tools provide means to better design the valve. In order to achieve a linear model, the flow force terms, which are dependent on both pressure and position, and the orifice equation, which depends on position and the square root of pressure, are linearized about a nominal valve position. Applying Taylor series expansion and neglecting higher order terms, the flow force terms of Eq. (2-1) and Eq. (2-2) can be approximated by Eq. (2-6).

$$flowforce \simeq (.72{C_d}^2 a_O)\Delta P + (.72{C_d}^2 h \bullet \Delta P_O) \bullet displacement$$

$$or \qquad flowforce \simeq kfc \bullet \Delta P + kfq \bullet displacement \tag{2-6}$$

It is noted that *displacement* represents the distance the poppet has moved from its nominal position while a_0 and P_0 represent conditions while the valve is at the nominal position. A Taylor series expansion of the classic orifice equation results in the linear approximation shown in Eq. (2-7).

$$Q \simeq \tfrac{1}{2} Q_O + \left(\frac{a_0 C_d}{\sqrt{2\rho \bullet \Delta P_O}} \right) \bullet \Delta P + \left(h C_d \sqrt{\tfrac{2}{\rho} \Delta P_O} \right) \bullet displacement$$

$$or \quad Q \simeq \tfrac{1}{2} Q_O + kc \bullet \Delta P + kq \bullet displacement \tag{2-7}$$

Substituting Eq. (2-6) into Eq. (2-1) and Eq. (2-2) while using nominal definitions for displacements results in Eq. (2-8) and Eq. (2-9) respectively.

$$M\ddot{y} = -b_y \dot{y} - k(y_n + x_n) - kfq_3 y_n + kfc_3 P_L + P_L A_L - P_C A_C + P_s A_s - kfc_3 P_s - k(x_O + y_O + preload) \tag{2-8}$$

$$m\ddot{x} = -B_x \dot{x} - k(y_n + x_n) - kfq_2 x_n - kfc_2 (P_C - P_L) + F - k(x_O + y_O + preload) \tag{2-9}$$

Changes in the size of the control volume will be neglected due the relatively small displacements of *y* and *x* respectively. Substituting Eq. (2-7) into Eq. (2-3) and Eq. (2-4) while assuming a nominal control volume results in Eq. (2-10) and Eq. (2-11).

$$\dot{P}_C = \frac{\beta}{V_{CO}} \left\{ A_c \dot{y} - kq_2 x_n - kc_1 P_C - kc_2 (P_C - P_L) + \tfrac{1}{2} (Q_{1O} - Q_{2O}) + kc_1 P_s \right\} \tag{2-10}$$

$$\dot{P}_L = \frac{\beta}{V_L} \left\{ kq_2 x_n + kq_3 y_n + kc_2 (P_C - P_L) - kc_3 P_L - kc_4 (P_L - P_T) + kc_3 P_s + \tfrac{1}{2} (Q_{2O} + Q_{3O} - Q_{4O}) \right\} \tag{2-11}$$

After choosing geometry, establishing a spring constant, and determining supply and tank pressures it is possible to calculate nominal pressures and hence to calculate the coefficients needed for the linear flow and flow force equations. Under nominal conditions the main poppet only has static forces acting on it and hence, neglecting flow forces, Eq. (2-1) reduces to Eq. (2-12).

$$P_{CO} = \frac{P_s A_s + P_{LO} A_L - k(x_O + y_O + preload)}{A_C} \tag{2-12}$$

Equation (2-2) reduces to Eq. (2-13) where F is an arbitrary input to be chosen

depending on the nominal position one wishes to study.

$$F = k(x_O + y_O + preload) \tag{2-13}$$

Static equilibrium of the each poppet also dictates that flow in equals flow out. Examining the control volume gives $Q_1 = Q_2$, which after simplification becomes:

$$P_{LO} = P_{CO} - \left(\frac{a_{1\,fix}}{a_{2O}}\right)^2 (P_s - P_{CO}) \tag{2-14}$$

Examining the load orifice gives $Q_2 + Q_3 = Q_4$, which after simplification becomes:

$$P_{LO} = \frac{{a_2}^2 P_{CO} + {a_{3O}}^2 P_s + {a_{4\,fix}}^2 P_T}{{a_{2O}}^2 + {a_{3O}}^2 + {a_{4\,fix}}^2} \tag{2-15}$$

Given that $a_{2O} = x_O h_2$ and $a_{3O} = y_O h_3$ there are only four unknowns, $(P_{CO}, P_{LO}, x_O, y_O)$, allowing Eq. (2-12) through Eq. (2-15) to be solved and the coefficients for the linear model to be determined.

CHAPTER 3

ITERATIVE ROOT LOCUS ANALYSIS AND DESIGN

3.1 Iterative Design Procedure:

Although the linearization in Chapter 2 requires geometry to be established, a goal of this research is to use linear design tools to establish geometric and other parameters that enhance valve performance. In order to achieve this, an iterative procedure is utilized in which an initial linear model is created and root locus plots serve as a guide to improving valve parameters. The preliminary model is developed from flow requirements, basic physics, and trial and error from nonlinear simulations until functional linearizations and root locus plots are created. Root locus plots for various parameters, valve openings, and pressure drops must be examined together and then a decision is made on which parameter(s) to change in attempts to improve the stability, speed, and damping of the system. After a constraint is changed, results can be examined with nonlinear simulations and new linearizations can be created. New linearizations give rise to a new set of root locus plots and the procedure is repeated until valve performance meets necessary objectives.

To begin the iterative procedure the linearized system is rewritten in state

space form so as to be conducive to creating root locus plots. Removing all terms from Eq. (2-8) through Eq. (2-11) which do not contain dynamic variables or the input force results in equations which represent deviations from the nominal conditions. The final deviation equations can be written in state-space form as presented in Eq. (3-1).

$$\dot{\bar{X}} = \begin{bmatrix} 0 & 1 & 0 & 0 & 0 & 0 \\ \frac{(-k-kfq_3)}{M} & \frac{-b_y}{M} & \frac{-k}{M} & 0 & \frac{(kfc_3+A_L)}{M} & \frac{-A_c}{M} \\ 0 & 0 & 0 & 1 & 0 & 0 \\ \frac{-k}{m} & 0 & \frac{(-k-kfq_2)}{m} & \frac{-b_x}{m} & \frac{kfc_2}{m} & \frac{-kfc_2}{m} \\ \frac{\beta}{V_L}kq_3 & 0 & \frac{\beta}{V_L}kq_2 & 0 & \frac{-\beta}{V_L}(kc_2+kc_3+kc_4) & \frac{\beta}{V_L}kc_2 \\ 0 & \frac{\beta}{V_{co}}A_c & \frac{-\beta}{V_{co}}(kq_2) & 0 & \frac{\beta}{V_{co}}kc_2 & \frac{-\beta}{V_{co}}(kc_1+kc_2) \end{bmatrix} \bar{X} + \begin{bmatrix} 0 \\ 0 \\ 0 \\ 1/m \\ 0 \\ 0 \end{bmatrix} u \qquad where\ \bar{X} = \begin{bmatrix} \delta y \\ \delta \dot{y} \\ \delta x \\ \delta \dot{x} \\ \delta P_L \\ \delta P_C \end{bmatrix} \qquad u = \delta f \qquad (3\text{-}1)$$

A program is written that calculates the eigenvalues or roots of the “system matrix” while one parameter is varied within a loop. In particular, root locus plots are examined for the area of orifice one, the slopes for orifice two and three, the spring rate, and the damping coefficient on the pilot poppet. It is thought that poppet valve instabilities often arise when the main poppet is just cracked open and hence the bulk of linearizations are for conditions in which the main poppet is open a half a millimeter or less. In an attempt to uncover various performance problems with the valve, separate linearizations are created for different pressure scenarios including: $(P_s = 35MPa \quad \Delta P \approx 35MPa)$, $(P_s = 35MPa, \Delta P \approx 1MPa)$, $(P_s = 21MPa, \Delta P \approx 2.1MPa)$, and $(P_s = 2.1MPa, \Delta P \approx 1MPa)$ where $\Delta P = P_S - P_L$.

3.2 Root Locus Plots for the Constant Orifice Model:

Fig. 3.1 through Fig. 3.6 show root locus plots for linearizations where the

input force to the pilot poppet is 5 N and the pressure drop across the valve is approximately 2.1 MPa. The root locus moves towards the X with a triangle around it as the parameter value is increased. In Fig. 3.4 through Fig. 3.6 the two poles to the far left, which appear in Fig. 3.3, have been excluded as they were relatively stationary and their removal significantly improved graph readability.

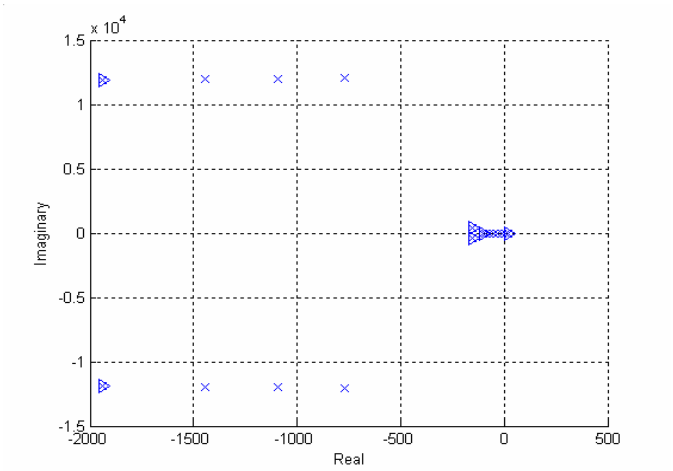

Fig. 3.1 Root locus varying a_1 (inlet orifice area), $(P_s = 21MPa, \Delta P \approx 2.1MPa)$ $f = 5N$

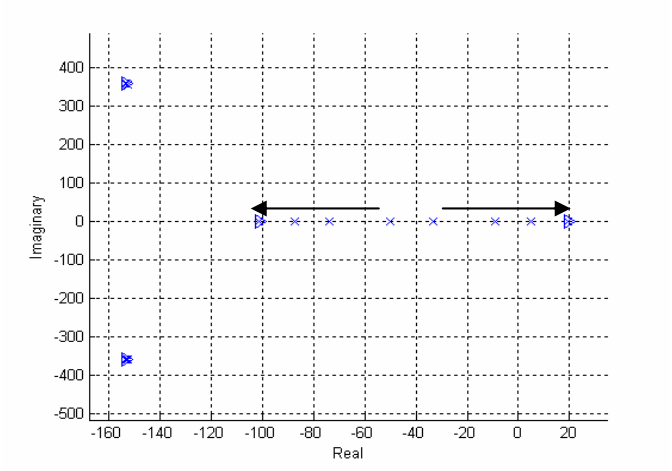

Fig. 3.2 Zoom of the right portion of Fig. 3.1

Fig. 3.1 and Fig. 3.2 demonstrate that of the parameters examined, a variation in

a_1 has the greatest impact on the position of the two left most poles as well as the right most pole. Fig. 3.3 shows that the slope of the main poppet orifice may have little impact on the systems poles while Fig. 3.4 establishes a connection between the slope of the pilot orifice and system oscillation. Fig. 3.5 reveals that if the spring rate is too low the valve will be unstable while if it is too high excessive oscillation can occur.

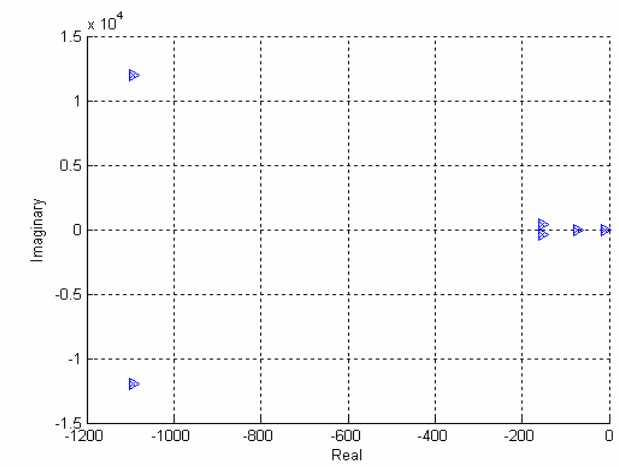

Fig. 3.3 Root locus varying h_3 (main orifice slope), $(P_s = 21MPa, \Delta P \approx 2.1MPa)$ $f = 5N$

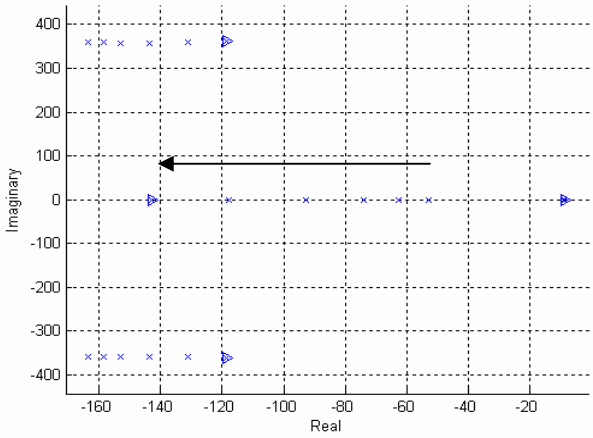

Fig. 3.4 Root locus varying h_2 (pilot orifice slope), $(P_s = 21MPa, \Delta P \approx 2.1MPa)$ $f = 5N$

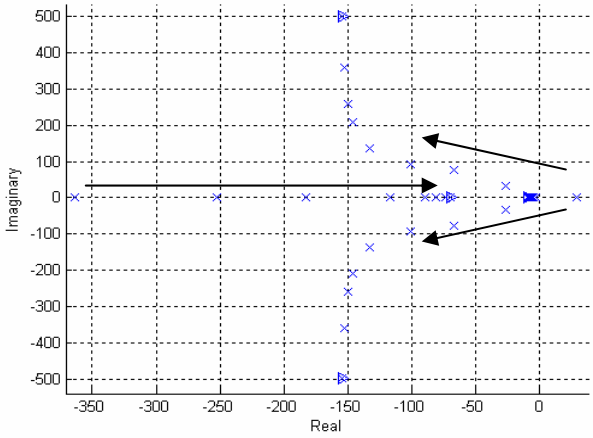

Fig. 3.5 Root locus varying k (spring rate), $(P_s = 21MPa, \Delta P \approx 2.1MPa)$ $f = 5N$

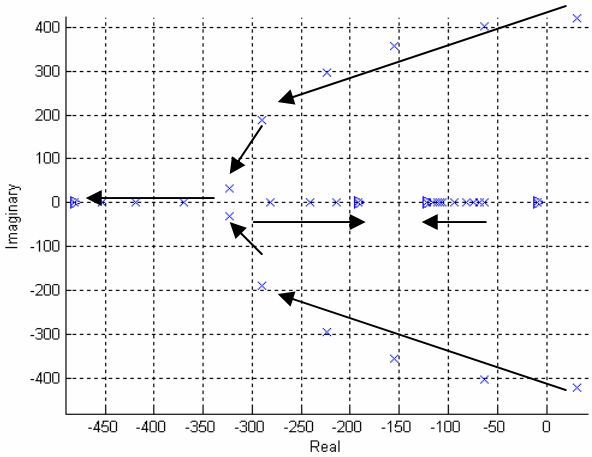

Fig. 3.6 Root locus varying b_x (pilot damping), $(P_s = 21MPa, \Delta P \approx 2.1MPa)$ $f = 5N$

Finally, Fig. 3.6 displays a correlation between the damping of the pilot poppet and the damping of the entire system. Caution is taken in making claims on valve performance based on Fig. 3.1 through Fig. 3.6 due to the fact these root locus plots originate from just one operating point. There is no reason to assume the valve will behave the same under more extreme pressure drops or larger nominal openings due to nonlinearity. Because of the large number of root locus plots needed to examine the valve in various scenarios, only a select few will be

shown to demonstrate contrasting information to what is shown in Fig. 3.1 through Fig. 3.6.

Careful examination of the root locus plots from various valve openings and pressure drops reveals that the complex roots and the left most real root, as seen in Fig. 3.1 through Fig. 3.6, appear almost identical for different valve openings when the pressure drop is held constant. Fig. 3.7 supports this statement by displaying similar root movement to that of Fig. 3.5 even though the valve is now open 3.5 mm instead of 0.5 mm. It should be noted that the root locus path clustered around -10 in Fig. 3.5 has shifted to the left in Fig. 3.7 and ends at approximately -180. Although five of the six roots appear nearly independent of valve position they shift dramatically and even take different shape as the pressure drop is varied. Fig. 3.8 is a root locus plot for the scenario depicted in Fig. 3.1 and Fig. 3.2 with the only change being an increase in pressure drop from 2.1 MPa to 35 MPa. Comparing these figures, one can see that an increase in pressure drop results in a dramatic shift of all root paths. Fig. 3.9 can be contrasted with Fig. 3.5 and demonstrates that a higher pressure drop results in a significantly different root locus plot as the spring constant is varied. Both figures link a higher spring rate to more oscillation but Fig. 3.9 also establishes that optimum performance at high pressure drops demands increasing the spring rate.

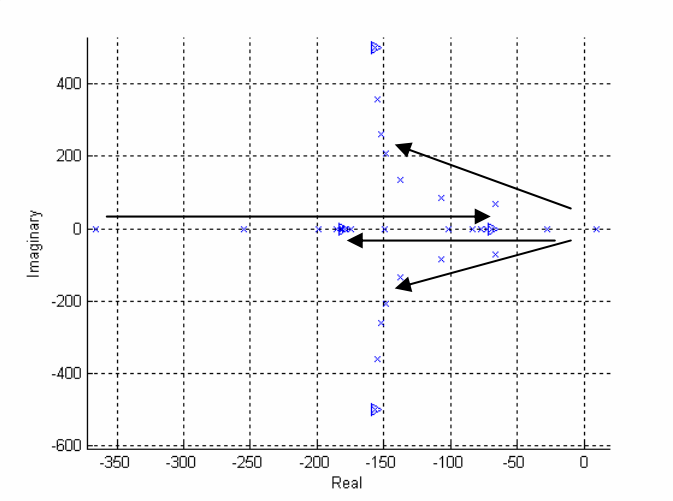

Fig. 3.7 Root locus varying *k* (spring rate), $(P_s = 21MPa, \Delta P \approx 2.1MPa)$ $f = 30N$

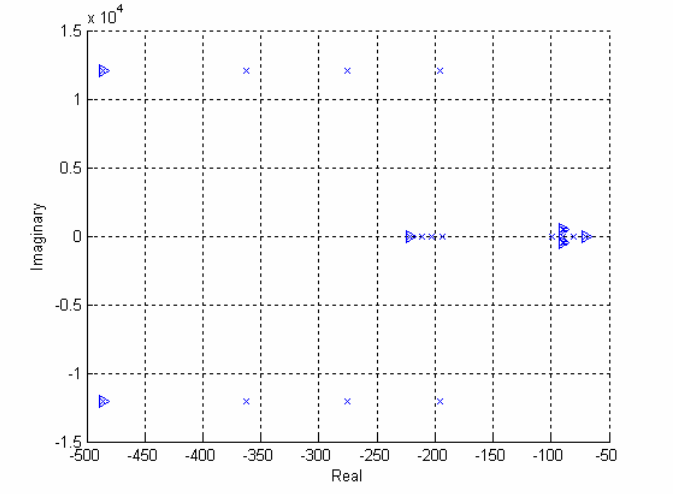

Fig. 3.8 Root locus varying a_1 (inlet orifice area), $(P_s = 35MPa \;\; \Delta P \approx 35MPa)$ $f = 5N$

The real root that is located at approximately -10, in Fig. 3.1 through Fig. 3.6, initially appears problematic as it hinders the system speed. The design variables tested do not provide a means to adequately position the pole, but a thorough examination of its movements reveals that this pole reflects the load dynamics or the fifth state equation.

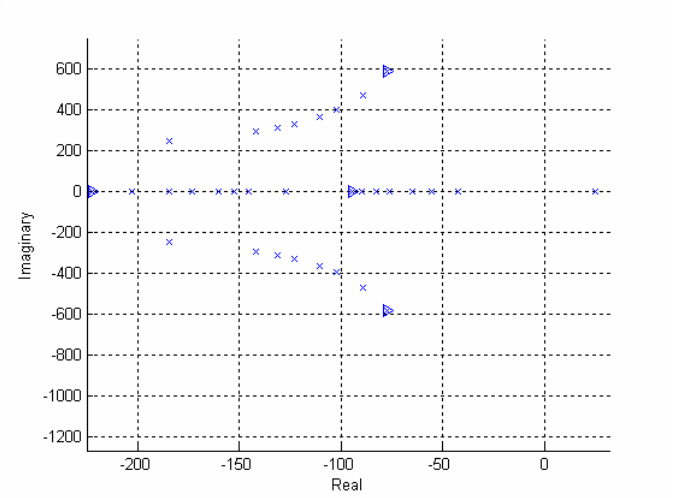

Fig. 3.9 Root locus varying k $(P_s = 35MPa \;\; \Delta P \approx 35MPa)$ $f = 5N$

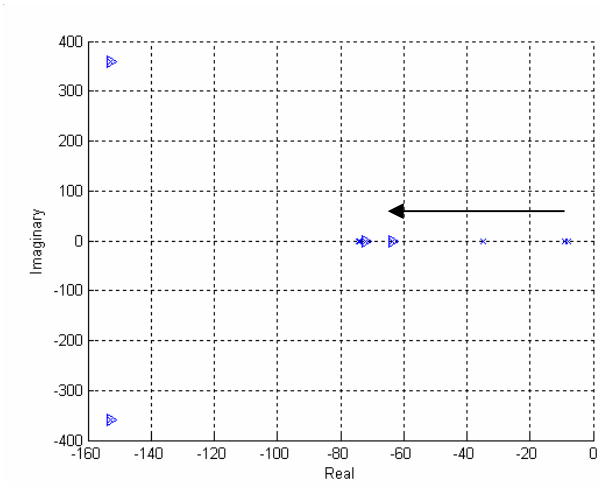

Fig. 3.10 Root locus varying kc_4 $(P_s = 21MPa, \Delta P \approx 2.1MPa)$ $f = 5N$

Fig. 3.10 brings light to the dominant effect kc_4 (pressure flow coefficient for the load orifice) has on the location of this pole. In Fig. 3.10 the right most pole moves from -10 to -63 as kc_4 increases. Although the root at -10 in Fig. 3.1 through Fig. 3.6 appears to make the system unacceptably slow, Fig. 3.10 suggests this may not be the case. kc_4 is dependent on the load orifice area

which has been arbitrarily adjusted to achieve desired pressure drops across the valve. The impact that kc_4 or the entire fifth state equation has on the system dynamics is also dependent on V_L (load volume) which again is an arbitrary value. This information suggests ignoring this pole in performance comparisons and indicates that the load model should be improved to examine its impact on stability. Due to the realized limitations of the load model presented in Chapter 2, Chapter 4 assumes load pressure is fixed while Chapter 5 further analyzes the impact of a varying load pressure.

CHAPTER 4

VARIABLE ORIFICE VS CONSTANT ORIFICE MODELS

4.1 Equations for the Variable Orifice Model:

The constant orifice model, given by Eq. (2-8) through Eq. (2-11), can be easily modified to create the variable orifice model, as shown in Fig. 1.1. Equation (2-8) and Eq. (2-11) remain unchanged. Equation (2-9) must have three additional terms to account for flow forces while Eq. (2-10) gains one term to account for decreasing flow into the control volume as the pilot poppet opens. It should be noted that both kq_1 and kfq_1 will be negative due to the negative relationship between *x* and the area of orifice one. The variable orifice model is then represented by Eq. (2-8), Eq. (2-11), Eq. (4-1), and Eq. (4-2).

$$m\ddot{x} = -B_x\dot{x} - k(y_n + x_n) - kfq_2 x_n + kfq_1 x_n - kfc_1 P_C - kfc_2(P_C - P_L) + F - k(x_O + y_O + preload) + kfc_1 P_s \quad (4\text{-}1)$$

$$\dot{P}_c = \frac{\beta}{V_{CO}}\left\{A_C\dot{y} + kq_1 x_n - kq_2 x_n - kc_1 P_C - kc_2(P_C - P_L) + \tfrac{1}{2}(Q_{1O} - Q_{2O}) + kc_1 P_s\right\} \quad (4\text{-}2)$$

4.2 Criteria for Constant Verses Variable Orifice Model Comparisons:

The iterative root locus procedure performed on the constant orifice model is also employed to analyze the variable orifice model although root locus plots are not shown. In order to make the clearest comparison between the constant

and variable orifice models, the scenarios presented in this chapter are designed so each model has nearly the same bandwidth. The models have identical values for the pilot damping term, B_x, and for the feedback spring rate, k. The value used for B_x is based on damping measurements from existing valves while k comes directly from root locus analysis. The slope on the main poppet orifice is set so as to achieve a 120 LPM flow rate for a 2.1 MPa pressure drop when the valve is fully open. Similar bandwidths are achieved by adjusting the geometry for the inlet and outlet orifices to the control volume. Fig. 4.1 presents the area functions of inlet and outlet orifices for both models.

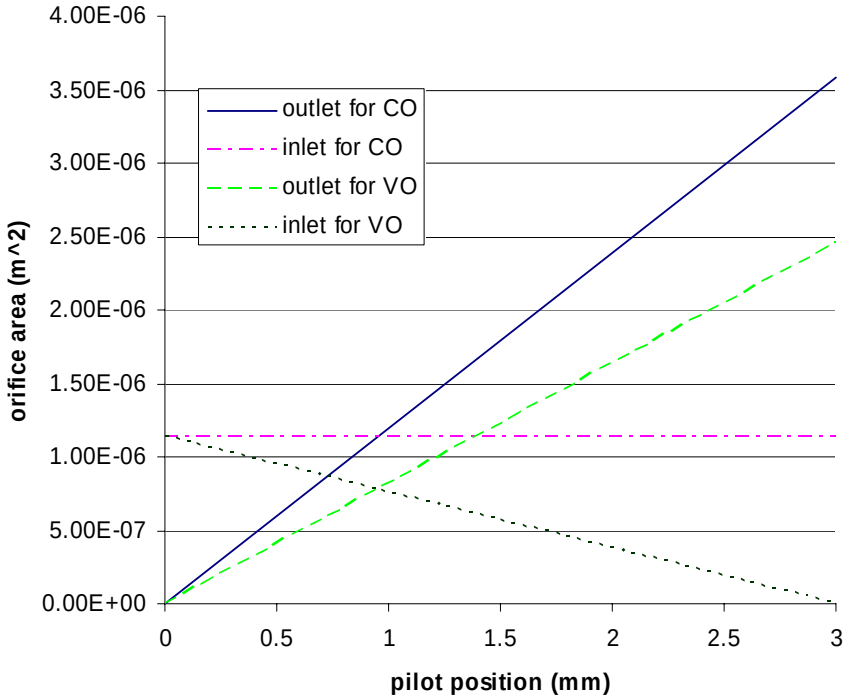

Fig. 4.1 Control volume inlet and outlet orifices

When the pilot poppet is closed both valves have the same inlet orifice area and when the pilot poppet is fully open their outlet area minus their inlet area is also

equal. It is important to note that in each case the pilot poppet has a deadband of approximately 1 mm before the outlet area will become larger than the inlet area. Fig. 4.2 displays the roots for both systems with load pressure fixed and a 2.1 MPa pressure drop across the valve, while Fig. 4.3 zooms in on the right portion of Fig. 4.2.

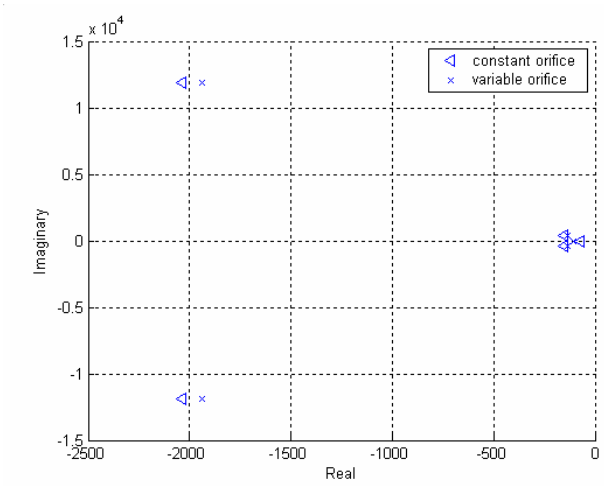

Fig. 4.2 Roots for linearization with 2.1 MPa pressure drop and valve open 0.2 mm

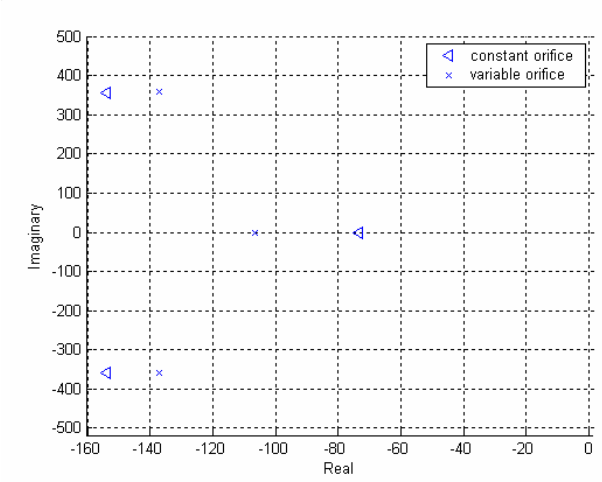

Fig. 4.3 Zoom in for the roots on the right side of Fig. 4.2

The Bode diagram appearing in Fig. 4.4 is from nonlinear simulations of the main

poppet position. The solenoid input force is a sinusoid such that the low frequency amplitude is 50% of the maximum poppet stroke. The system bandwidth is approximately 11.7 and 12.5 Hz for constant and variable orifice models respectively when the supply pressure is 21MPa and the load pressure is 20 MPa. Although it is not shown here, the bandwidth increases as the pressure drop across the valve increases.

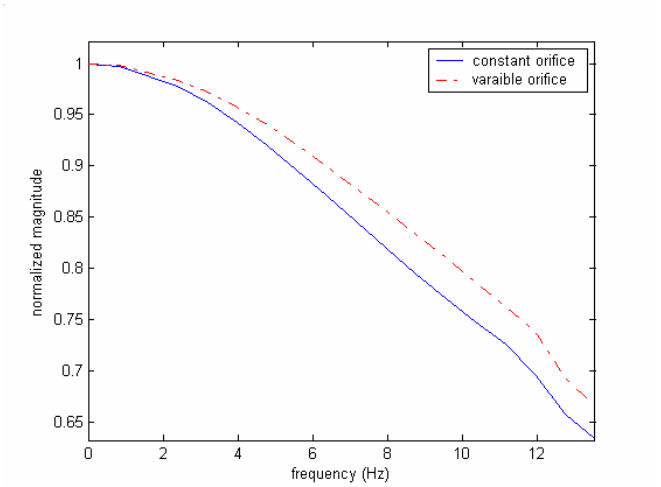

Fig. 4.4 Frequency response for both models ($P_s = 21MPa, \Delta P = 1MPa$)

4.3 Simulation Comparisons:

Fig. 4.5 displays the main poppet position for a step input force which is applied from 0 to 0.2 seconds. This figure demonstrates that for extremely low pressure drops the main poppet can open or close 6 mm in approximately 0.075 seconds. The response is well damped and shows no signs of instability. An entirely different response appears in Fig. 4.6 when the pressure drop is increased to 35 MPa. Both models result in overshoot and oscillation, but oscillations for the constant orifice model do not drop off as quickly. It is also

interesting to note that the input force required to open the valve 6 mm has changed significantly from that of Fig. 4.5.

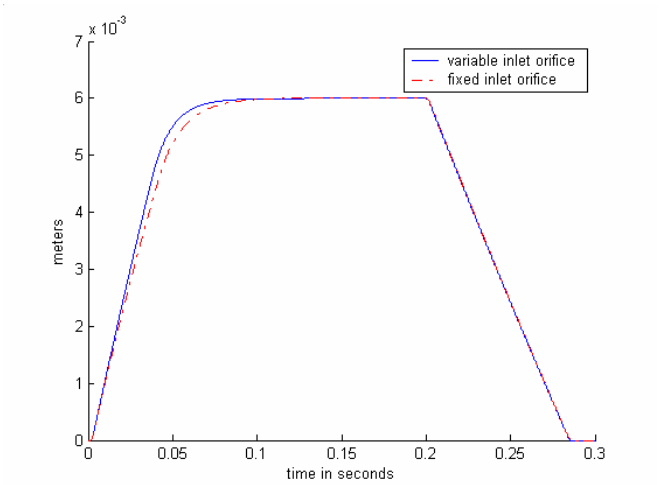

Fig. 4.5 Main poppet position in response to step input force from 0-.2 s, F=50.2 N for variable orifice, F= 51.4 for constant orifice ($P_s = 2.1MPa, \Delta P = 1MPa$)

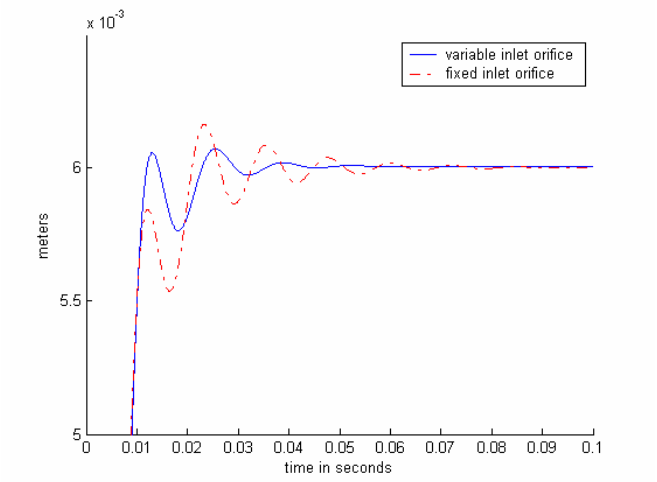

Fig. 4.6 Main poppet position in response to step input force, F=48.8 N for variable orifice, F= 54.6 for constant orifice ($P_s = 35MPa, \Delta P \approx 35MPa$)

The primary explanation for the differences in input force required to open the valve is linked to the flow force terms included in the model. As was stated

previously, the flow forces are dependent on pressure drop and orifice area, and are assumed to act in a direction to close the given orifice. For the constant orifice model, outlet flow from the control volume results in a force to close the pilot poppet which the solenoid must act against. This means that as the pilot opens further or as the pressure drop increases, the flow forces grow and so must the solenoid force. The geometry choices of Fig. 4.1 establish that there will always be more flow through outlet orifice of the constant orifice model for a given pressure drop and valve opening. Fig. 4.7 presents the flows out of the control volume for the main poppet responses of Fig. 4.6.

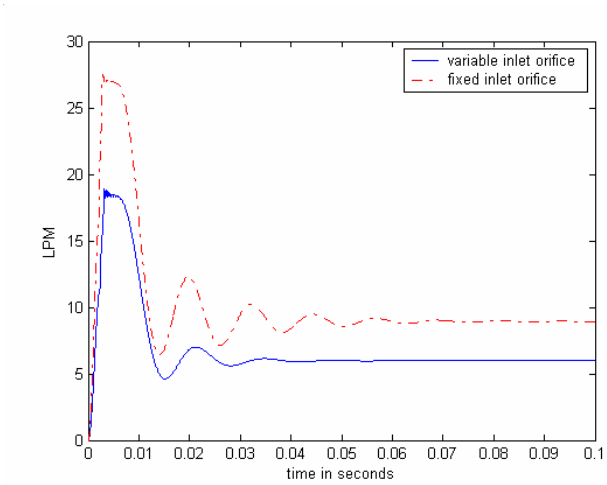

Fig. 4.7 Flow out of the control volume for main poppet response of Fig. 4.6 ($P_s = 35MPa, \Delta P \approx 35MPa$)

In the case of the variable orifice model, there are two orifices having an impact on the pilot poppet. The inlet orifice acts to open the pilot poppet while the outlet orifice acts to close it. Due to this representation, the flow forces are partially cancelled and are thought to help stabilize the pilot poppet. Fig. 4.8

demonstrates that overshoot and oscillation problems can be even more exaggerated for the case when the main poppet is cracked less than 1 mm.

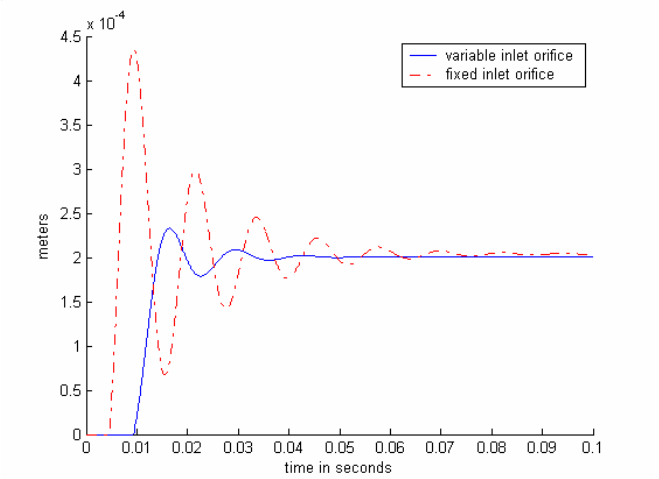

Fig. 4.8 Main poppet cracked open in response to step input force, F=8.1 N for variable orifice, F=13.6 N for constant orifice $(P_s = 35MPa, \Delta P \approx 35MPa)$

4.4 Design Information Obtained from Model Comparisons:

Nonlinear simulations show that constant and variable orifice models can be designed to have similar bandwidths, but there are trade offs between the two models. In order to obtain similar bandwidths, the constant inlet orifice had to be enlarged so it was equal to the maximum size of the variable inlet orifice and the slope of the outlet orifice had to be increased in the constant orifice model. Fig. 3.2 indicates that performance can be reduced if the area of the inlet orifice is set too large while Fig. 3.4 suggests that if the outlet orifice slope is too steep oscillation may be a problem. Although it is not possible to determine direct cause and effect, nonlinear simulations of Fig. 4.6 and Fig. 4.8 show increased oscillation for the constant orifice model. In short, the constant orifice model forces a compromise between designing for a stability margin and for system

bandwidth. In Fig. 4.1 through Fig. 4.8 the design focused on bandwidth while Fig. 4.9, Fig. 4.10, and Fig. 4.11 show a constant orifice model design which is focused on stability. These figures pertain to a model that has an outlet orifice slope equal to that of the variable orifice model and the fixed inlet orifice which has been reduced to 4.375e-7 m^2. Fig. 4.9 demonstrates how a reduction in the inlet orifice area can slow the closing of the main poppet. This increase in the valve close time is due to a reduction of the pressure rise rate for the control volume. When the solenoid is shut off, the spring force quickly closes the pilot poppet, but the main poppet will not close immediately. The spring force is not strong enough to counter the upward force on the main poppet due to supply pressure.

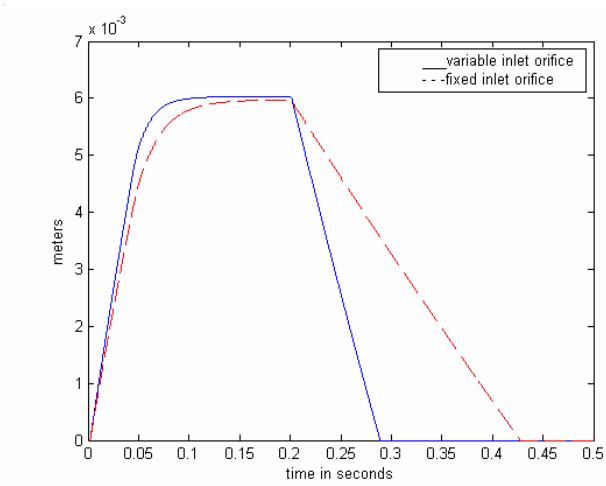

Fig. 4.9 Main poppet response to a solenoid input force from 0-.2 s. Constant orifice model modified for stability as compared to Fig. 4.5 ($P_s = 2.1MPa, \Delta P = 1MPa$)

The pressure in the control volume must increase enough to force the main poppet closed. This pressure rise rate is dependent on the size of the inlet orifice and hence why a reduction in the inlet area impacts valve closing. It is

noted that the simulation in Fig. 4.9 is with a low pressure drop for the purpose of examining the worse case scenario. At higher pressure drops the variable orifice model continues to out perform the constant orifice model but with a decreasing margin. Although Fig. 4.9 represents a decrease in performance it was also claimed that geometry changes would trade performance for stability.

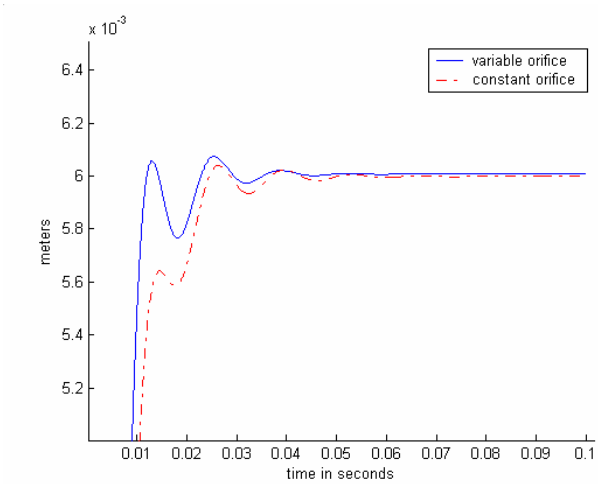

Fig. 4.10 Main poppet response to solenoid input force. Constant orifice model modified for stability as compared to Fig. 4.6 ($P_s = 35MPa, \Delta P \approx 35MPa$)

Fig. 4.10 backs this claim by showing that the adjustments to the constant orifice model reduced both oscillation and overshoot below that of the variable orifice model. Finally, Fig. 4.11 presents the change in system bandwidth that results from attempts to increase the stability margin of the constant orifice model. In particular it is shown that the bandwidth drops from approximately 11.7 to 6 Hz.

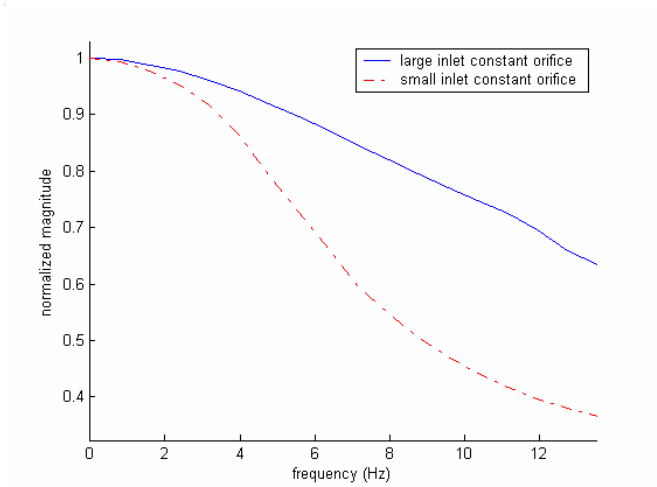

Fig. 4.11 Frequency response for both versions of the constant orifice model ($P_s = 21MPa, \Delta P = 1MPa$)

CHAPTER 5

EXAMINATION OF PREVIOUSLY UNMODELED DYNAMICS

5.1 An 8-State Model:

Bode plots and nonlinear simulations, presented in Chapter 3 and Chapter 4, compare constant and variable orifice models for five-state systems, while the original root locus plots depended on a 6-state model. Although useful comparative results could be extracted, it is important to expand the system to examine the validity of the assumptions made. In particular, this chapter will study the effects of improved load dynamics and nonlinear damping on the pilot poppet. The original load orifice will be replaced with a piston/cylinder assembly and the artificial linear damping of the pilot poppet will be replaced by pressure forces acting on its ends and flow through its central tube. The new model will contain eight states: the main poppet position and velocity ($y, \dot{y}$), the pilot poppet position and velocity ($x, \dot{x}$), the control volume pressure between the two poppets (P_C), the control volume pressure above the pilot poppet (P_P), the load volume pressure (P_L), and the velocity of the load piston ($\dot{z}$). The main control volume is connected to the pilot poppet control volume via the tube located in the center of the pilot poppet. It is assumed that classic laminar tube flow will exist

between the two control volumes as presented in Eq. (5-1).

$$Q_6 = \frac{\pi R^4}{8\mu L_{pilot}}(P_C - P_P) \tag{5-1}$$

The artificial damping term, B_x, is replaced by a more realistic linear damping coefficient, b_x. In linearizing the model, the assumption is made that variations in each control volume size can be neglected. The piston/cylinder assembly is modeled as a simple mass-damper system with load pressure acting on the head end of the piston and an external load force acting on the rod end. In this scenario, the load force, F_{load}, can be adjusted to provide desired pressure drops across the valve. Both the constant and variable orifice models are expanded to eight states although the results are only shown for the variable orifice model. It is also important to note that from Chapter 5 onward, all results presented will make use of an 8-state model with the parameters given in the appendix. Equation (5-2) through Eq. (5-7) represent the nonlinear variable orifice model while Eq. (5-8) represents the linear equations written in state space form.

$$M\ddot{y} = -b_y\dot{y} - k(y + x + preload) - P_C A_C + P_s A_s + P_L A_L - .72C_d{}^2 h_3 y(P_s - P_L) \tag{5-2}$$

$$\begin{aligned} m\ddot{x} = {} & -b_x\dot{x} - k(y + x + preload) - A_{pilot}(P_C - P_p) \\ & + .72C_d{}^2(h_1 x + a_{1\max})(P_s - P_C) - .72C_d{}^2 h_2 x(P_C - P_L) + F \end{aligned} \tag{5-3}$$

$$\dot{P}_c = \frac{\beta}{V_C - A_C y}(Q_1 - Q_2 + A_c\dot{y}) \tag{5-4}$$

$$\dot{P}_P = \frac{\beta}{V_{pilot} + A_{pilot} x}(Q_6 - A_{pilot}\dot{x}) \tag{5-5}$$

$$\dot{P}_L = \frac{\beta}{V_{Load} + A_{pist} z}(Q_2 + Q_3 - A_{pist}\dot{z}) \tag{5-6}$$

$$M_{pist}\ddot{z} = P_L A_{pist} - b_z \dot{z} + F_{load} \tag{5-7}$$

$$\dot{\bar{X}} = \begin{bmatrix}
0 & 1 & 0 & 0 & 0 & 0 & 0 & 0 \\
\frac{-k - kfq_3}{M} & \frac{-b_y}{M} & \frac{-k}{M} & 0 & \frac{-A_c}{M} & 0 & \frac{kfc_3 + A_L}{M} & 0 \\
0 & 0 & 0 & 1 & 0 & 0 & 0 & 0 \\
\frac{-k}{m} & 0 & \frac{-k - kfq_2 + kfq_1}{m} & \frac{-b_x}{m} & \frac{-kfc_1 - kfc_2 - A_{pilot}}{m} & \frac{A_{pilot}}{m} & \frac{kfc_2}{m} & 0 \\
0 & \frac{\beta}{V_{C0}} A_C & \frac{\beta}{V_{C0}}(kq_1 - kq_2) & 0 & \frac{-\beta}{V_{C0}}(kc_1 + kc_2) & 0 & \frac{\beta}{V_{C0}} kc_2 & 0 \\
0 & 0 & 0 & \frac{-\beta}{V_{P0}} A_{pilot} & \frac{\beta}{V_{P0}} kcp & \frac{-\beta}{V_{P0}} kcp & 0 & 0 \\
\frac{\beta}{V_{L0}} kq_3 & 0 & \frac{\beta}{V_{L0}} kq_2 & 0 & \frac{\beta}{V_{L0}} kc_2 & 0 & \frac{-\beta}{V_{L0}}(kc_2 + kc_3) & \frac{\beta}{V_{L0}} A_{pist} \\
0 & 0 & 0 & 0 & 0 & 0 & \frac{A_{pist}}{M_{pist}} & \frac{-b_z}{M_{pist}}
\end{bmatrix} \bar{X}$$

$$+ \begin{bmatrix} 0 \\ 0 \\ 0 \\ 1/m \\ 0 \\ 0 \\ 0 \\ 0 \end{bmatrix} u \qquad \bar{X} = \begin{bmatrix} \delta y \\ \delta \dot{y} \\ \delta x \\ \delta \dot{x} \\ \delta P_C \\ \delta P_P \\ \delta P_L \\ \delta \dot{z} \end{bmatrix} \qquad u = \delta f \tag{5-8}$$

5.2 Validation of 8-State Model Linearization:

The linear model of Eq. (5-8) is not only used to verify claims made with the 5-state model, but is also used in Chapter 6 in efforts to create a system observer. The accuracy of an observer depends on accuracy of the model it employs. For this reason and as a general check on mathematical efforts thus far, simulations are run side by side for both the linear and nonlinear models. Fig. 5.1 through Fig. 5.8 show that the linear model provides an excellent approximation of the nonlinear model for all 8 states in response to a unit step input.

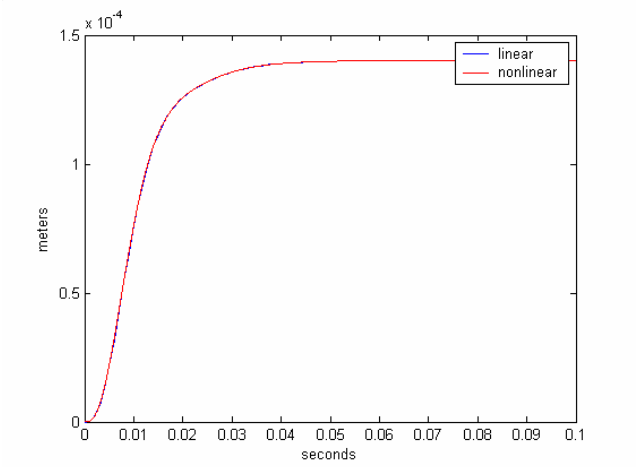

Fig. 5.1 Main poppet position for a unit step input

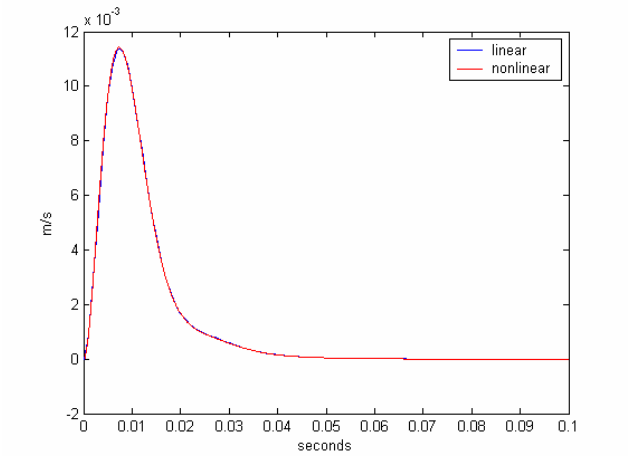

Fig. 5.2 Main poppet velocity for a unit step input

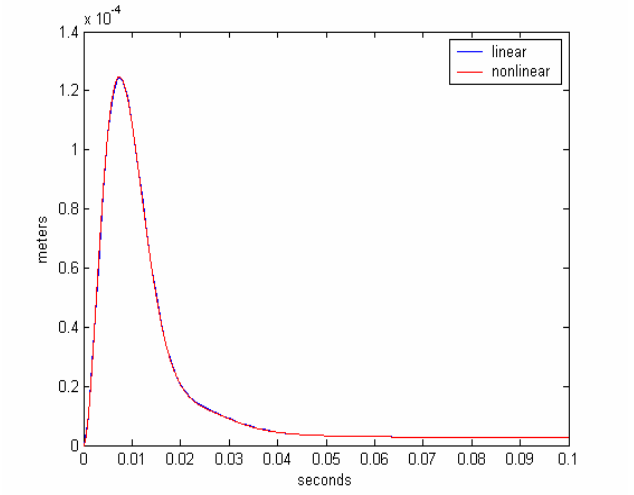

Fig. 5.3 Pilot poppet position for a unit step input

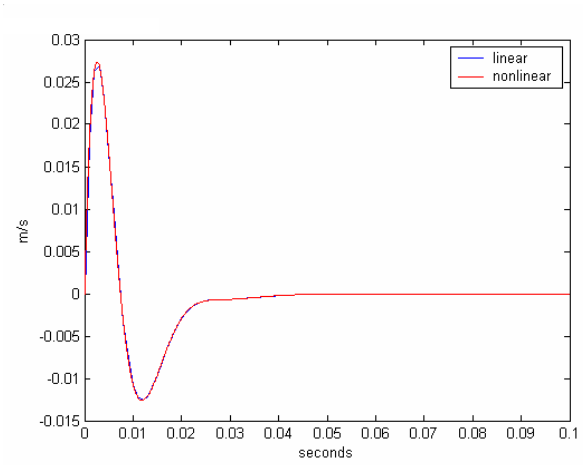

Fig. 5.4 Pilot poppet velocity for a unit step input

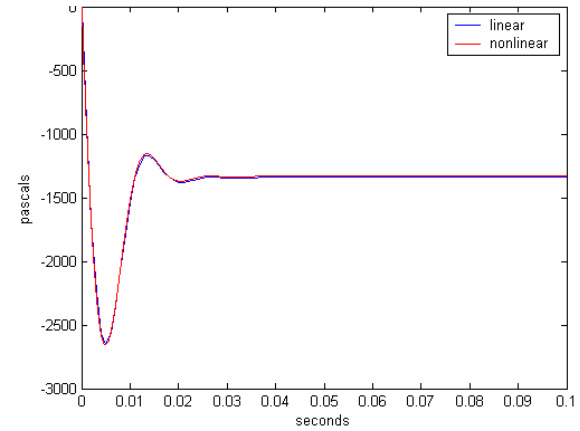

Fig. 5.5 Control volume pressure for a unit step input

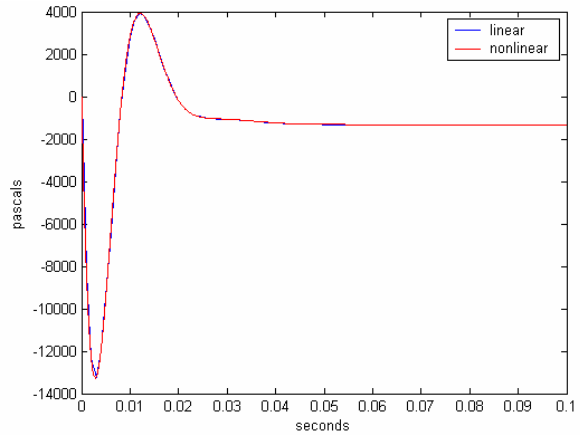

Fig. 5.6 Pilot control volume pressure for a unit step input

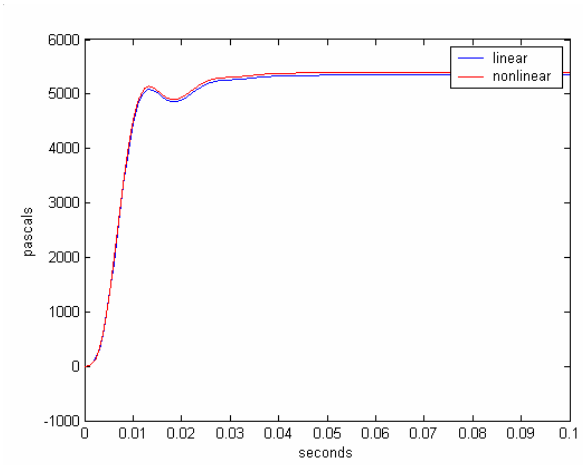

Fig. 5.7 Load volume pressure for a unit step input

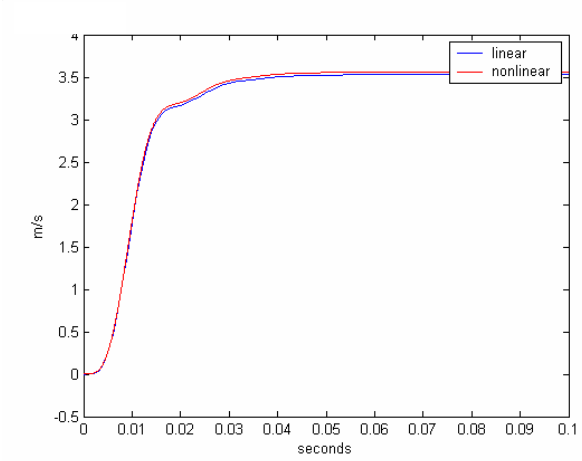

Fig. 5.8 Load piston velocity for a unit step input

5.3 8-State vs. 5-State Model:

In Chapter 3 a decision was made to replace a restrictive load orifice model with a fixed load pressure. The assumption was made that arbitrary settings on both the load orifice and load volume were introducing an extraneous root at -10. Fig. 5.9 displays the roots of the expanded system and the 5-state system for a 2.1 MPa pressure drop. It is noted that the extremely fast root (-326,000) associated with P_P has been removed from the graph for readability.

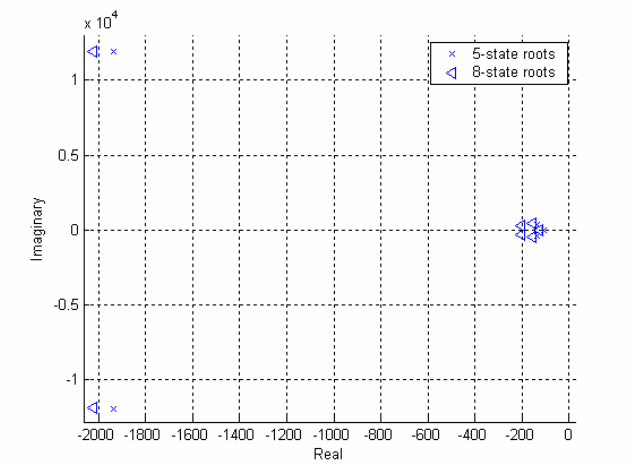

Fig. 5.9 Roots for linearization with valve open 0.2 mm ($P_s = 21MPa, \Delta P \approx 2.1MPa$)

Fig. 5.10 provides more information about how the poles have moved between the 5-state and 8-state models. In general the 8-state model appears to have faster roots but careful analysis determines that the imaginary poles at $-155 \pm 463i$ are due to the variable load pressure and the load piston dynamics. While the load pressure is not creating an extremely slow root at -10 as early results suggested, Fig. 5.10 suggests that load dynamics can impact system performance and stability.

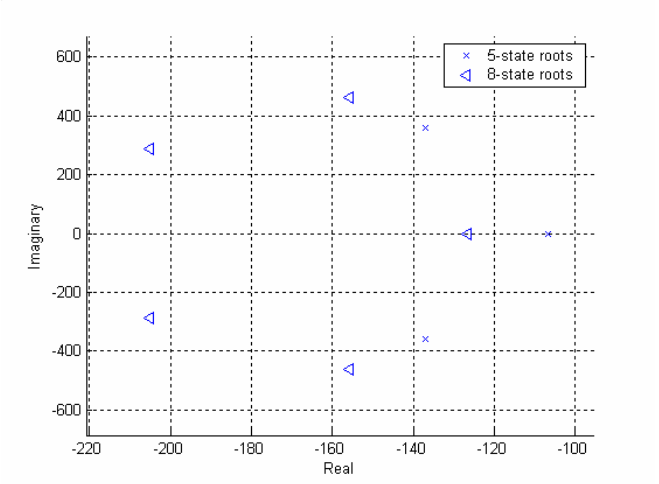

Fig. 5.10 Zoom in for the right side of Fig. 5.9

Again, it is imperative to remember that poles presented here are for a linearization at only one set of operating conditions. Although not shown here, nonlinear simulations and linearizations for an array of operating conditions support that the system is stable with nonlinear damping and tube flow through the pilot poppet. Examination of the Reynolds number for flow through the pilot poppet does show spikes above 2100 which is in violation of Eq. (5-1) [16]. The spikes in the Reynolds number occur when the pilot poppet rapidly accelerates from a zero velocity due to the solenoid or spring forces. It is possible that flow will transition from laminar to turbulent, and that the pilot poppet will not move as quickly as the model indicates. The assumption is made that this will not seriously degrade system performance and that the model captures the important dynamics.

The 8-state model predicts, as is expected, that system performance is degraded under extreme load forces or low pressure drops while it shows more oscillation at high pressure drops. In order to validate that the 8-state model meets performance requirements, Fig. 5.11 again presents a Bode plot created from nonlinear simulations.

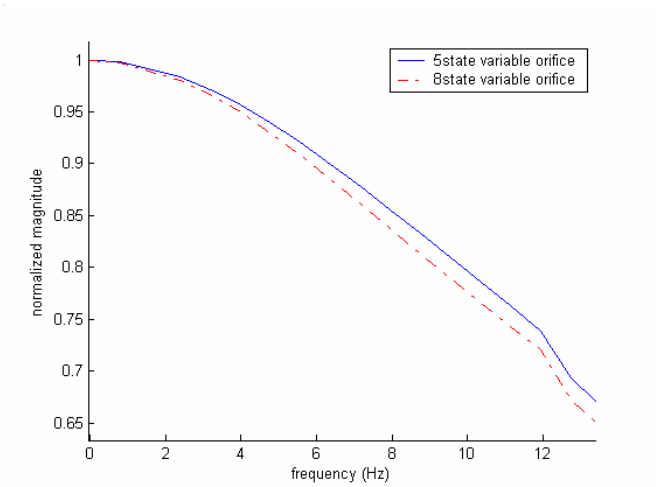

Fig. 5.11 Frequency response for both versions of the constant orifice model ($P_s = 21MPa, \Delta P = 1MPa$)

These results suggest that a variable load pressure as opposed to a fixed load pressure has only a small impact on the system bandwidth. As a whole, the results from the 8-state model indicate that the 5-state model includes the important performance characteristics of the system but neglects stability concerns that may arise from the interaction with load dynamics.

CHAPTER 6

MECHANICAL AND ELECTRONIC CONTROL DESIGNS

6.1 Introduction to Flow Control:

The first phase of this research was to design a forced-feedback metering poppet valve which meets open loop performance requirements for the main poppet position. The second phase focuses on methods to control flow across the valve. Flow is dependent on both poppet position and pressure drop across the valve which leads to two methods for achieving flow control. The first method is to use a mechanical pressure compensator to maintain a desired pressure drop across the valve while the operator adjusts the poppet position as needed to provide the desired flow. Although valve design shown in Fig. 1.1 and Fig. 1.2 provides no means to attach a compensator, mathematical modeling makes the assumption that it is possible. The second method of flow control is to allow pressure drop to vary freely and then establish the poppet position as a function of both desired flow and measured pressure drop. This method entails the use of electronic control and feedback of pressure drop across the valve. Several electronic control designs will be presented while mechanical pressure compensation will serve as a benchmark for performance.

6.2 Mechanical Pressure Compensation for Flow Control:

The mechanical pressure compensator is a pre-compensator with a restriction on supply side pressure. The model consists of a typical spring mass damper system which affects the size of a variable orifice between supply pressure, P_s, and the compensated supply pressure, $P_{s,c}$.

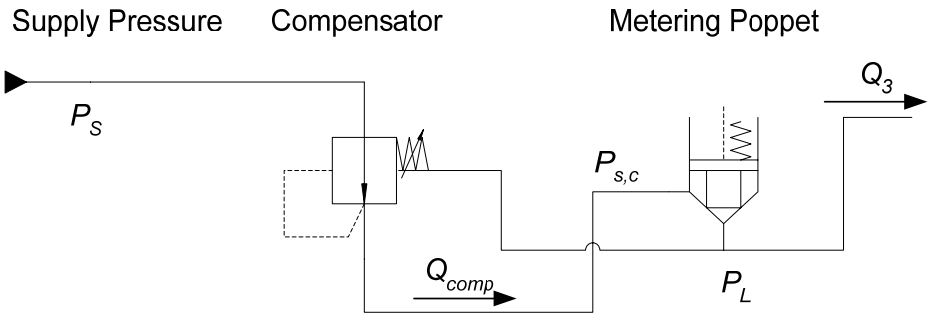

Fig. 6.1 System with compensator, metering poppet valve, and load

The compensator is implemented in the system as shown in Fig. 6.1 while it is mathematically represented by Eq. (6-1), Eq. (6-2), and Eq. (6-3).

$$m_{comp}\ddot{x}_{comp} = k_{comp}x_{comp} - b_{comp}\dot{x}_{comp} - P_L A_{comp} + P_{s,c}A_{comp} + F_{c,pre} \tag{6-1}$$

$$\dot{P}_{s,c} = \frac{\beta}{V_{comp}}(Q_{comp} - Q_3) \tag{6-2}$$

$$Q_{comp} = a_{comp}C_d\sqrt{\frac{2}{\rho}(P_s - P_{s,c})} \tag{6-3}$$

Assuming supply pressure is at least 2 MPa higher than load pressure, the compensator is designed to maintain approximately a 2 MPa pressure drop across the metering poppet valve. Fig. 6.2 displays nonlinear simulation results for both the constant and variable orifice models with pressure compensation. In

these simulations the input was set to achieve a desired flow of 30 LPM while supply pressure was constant and the load pressure varied as much as 1GPa/s. Fig. 6.3 is a profile of the difference between supply pressure and load pressure.

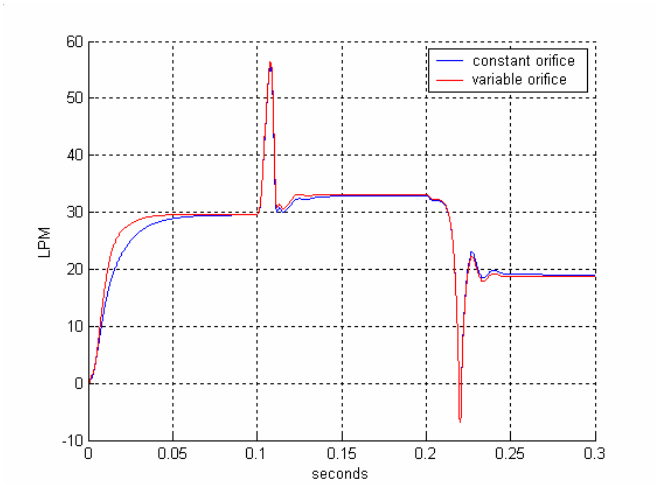

Fig. 6.2 Valve flow for pressure compensated models (desired flow 30LPM)

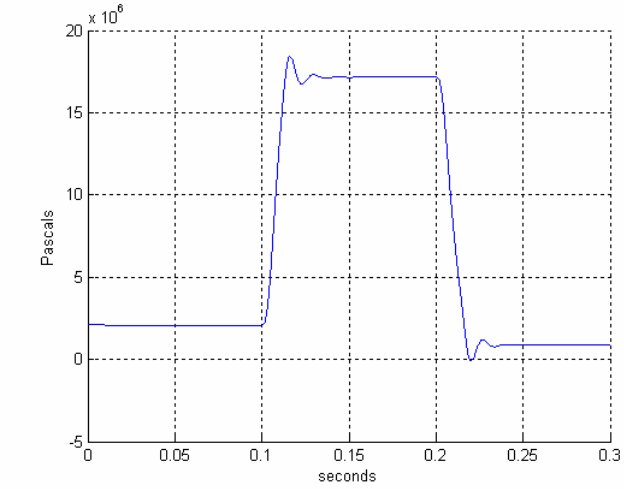

Fig. 6.3 Pressure drop from supply to load pressure

Fig. 6.2 provides expected results for mechanical pressure compensation. For the first 0.1 seconds the pressure drop is near 2MPa and therefore there is no pressure compensation. The variable orifice model settles to steady state slightly

faster than the constant orifice model in agreement with previous results. At 0.1 seconds the load pressure begins to fall approximately 1 GPa/s. The flow quickly spikes as the compensator lags behind but then settles to 33 LPM. When the load pressure rises at 0.2 seconds, the compensator again lags behind but opens fully and flow settles to 19 LPM. The final pressure drop is near 0.9 MPa which is below the compensators designed pressure drop and therefore high steady state error results. Due to the similar results between the two models, plots of electronic control schemes will only be contrasted with the compensated variable orifice model.

6.3 Electronic Flow Control:

6.3.1 Table Look-up Control:

The first electronic control design employs feedback of the pressure drop and a simple look-up table to establish the solenoid input force and is shown in Fig. 6.4.

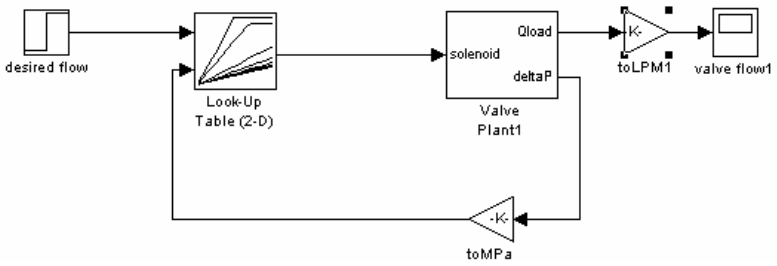

Fig. 6.4 Poppet valve control scheme with look-up table

The basic principle behind this controller is to calculate the necessary steady-state current to the solenoid based on desired flow and the measured pressure drop across the valve. In this case, knowledge of the model was used to make

approximate linear relationships between flow and solenoid force for a small array of pressure drops. The best controller of this type would be designed by creating a very precise look-up table based on actual tests of a sample of production valves. Fig. 6.5 and Fig. 6.6 provide nonlinear simulation results using the controller shown in Fig. 6.4. Simulations are run for desired flows of 30 and 110 LPM and the results are compared with mechanical pressure compensation. Again, it is noted that the constant orifice model as it appears in control design figures is the design which focuses on stability and not performance. For a 30 LPM flow, the simulation results appear similar although when the pressure drop becomes less than 2 MPa the mechanical compensator provides a much higher steady-state error.

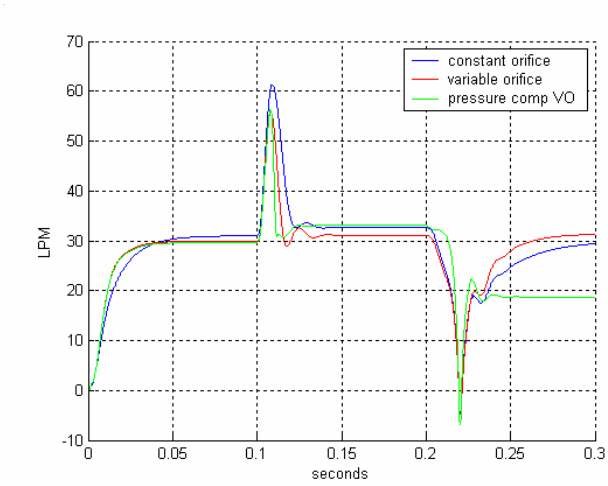

Fig. 6.5 Look-up table control vs. pressure compensation, desired flow 30 LPM, see Fig. 6.3 for pressure drop

The mechanical pressure compensator has no means to achieve the desired flow when the pressure drop falls below its design value while electronic control can open the valve further to minimize steady-state error. In Fig. 6.6 steady-state

error is similar even under low pressure drops because the valve eventually hits its endstop. The results for the transient response are significantly different for high flow compared to low flow. For a 30 LPM flow the percent overshoot is comparable for all models, while for 110 LPM flow, the pressure compensator provides a much smaller spike in flow in response to the sudden drop in load pressure.

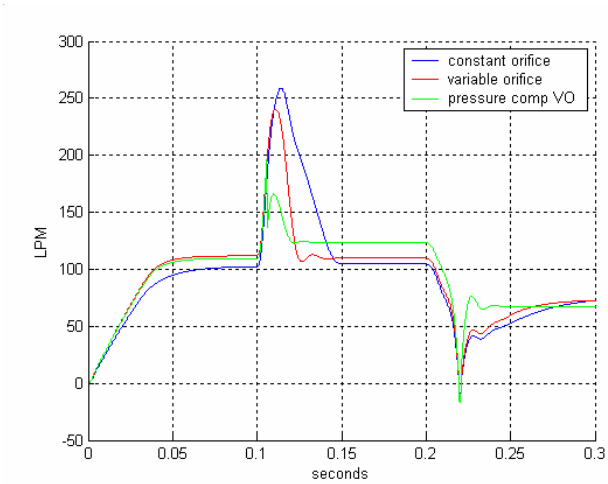

Fig. 6.6 Look-up table control vs. pressure compensation, desired flow 110 LPM, see Fig. 6.3 for pressure drop

Although Fig. 6.5 and Fig. 6.6 indicate that the constant orifice model has the highest percent overshoot this is not always the case. In Fig. 6.7 and Fig. 6.8 the desired flow is varied over time while the pressure drop is relatively stable. The load force is held constant at appropriate values so that pressure drop is near 30 MPa in Fig. 6.7 and 1 Mpa in Fig. 6.8. For high pressure drops the variable orifice model with table look-up control has the highest overshoot and oscillates more than the other models while the constant orifice model actually has the

fastest settling time. For low pressure drops, all models show over damped responses but the variable orifice model has the fastest settling time.

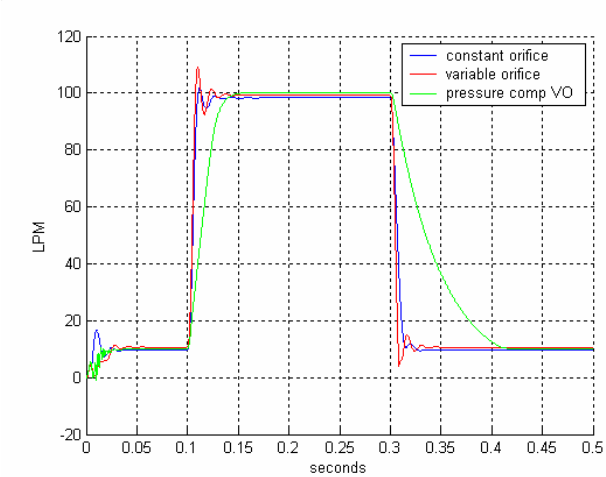

Fig. 6.7 Varying desired flow between 10 and 100 LPM, pressure drop approx 30MPa

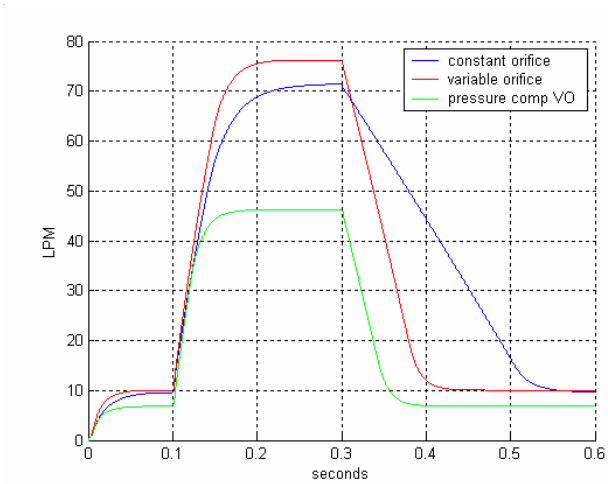

Fig. 6.8 Varying desired flow between 10 and 70 LPM, pressure drop approx 1 MPa

In general, as pressure drop decreases, the constant orifice model falls behind the performance of the variable orifice model. Control of the constant orifice model becomes limited by its poor open loop performance at low pressure drops. Steady-state error for electronic control models appears to vary more at low

pressure drops but this is direct result of simplifications in look-up tables. If the look-up tables are made more accurate, steady-state error should be identical for both models. Trade offs in using mechanical pressure compensation are demonstrated by its comparatively slower response at high pressure drops and its high steady state error at low pressure drops. High steady-state error is somewhat misleading in that an operator will intuitively provide a controlling response when the machine operates at this condition.

6.3.2 Table Look-up with PD Control:

The next electronic controller, shown in Fig. 6.9, seeks to enhance performance by combining look-up table control with proportional derivative (PD) control. It is noted that integrator control is not included in this work primarily due to slowness of response. Simulations which examined integrator control resulted in settling times that were typically more than an order of magnitude greater than when the integrator was not included. Because some steady-state error was deemed acceptable, work proceeded with only PD control.

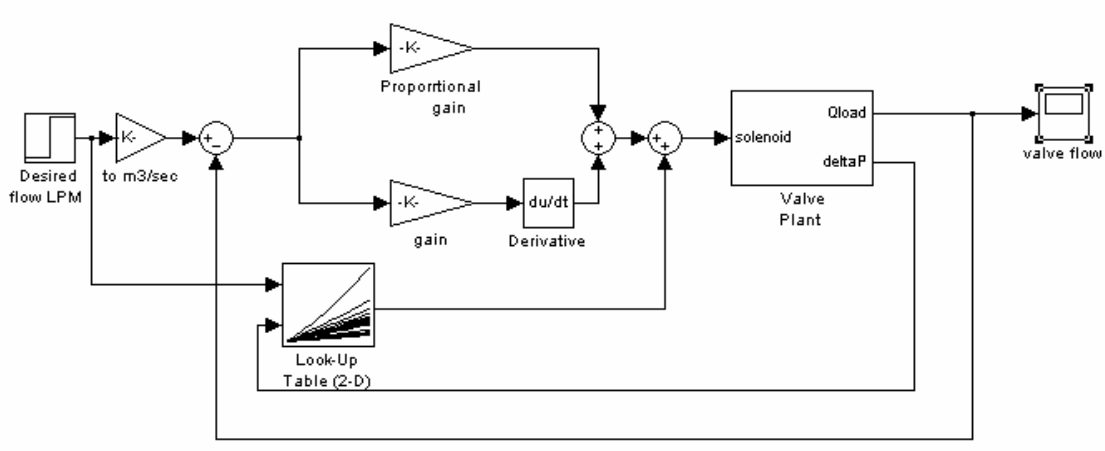

Fig. 6.9 Electronic control with look-up table and PD control

The controller shown in Fig. 6.9 feeds back pressure drop and valve flow. While pressure drop is still an input to the original look-up table, the flow feedback is used to establish a flow error signal which is incorporated into PD control. The proportional gain on the flow error signal can shorten the transient response while the derivative gain can be used to minimize overshoot. An additional benefit of this type of controller is that inaccuracies contained in the look-up table will be compensated for by gains on the flow error signal. Although a look-up table can be designed using test data, each valve will be unique and will perform differently as it shows wear. A drawback of using PD control on the flow error signal is that it requires having knowledge of the flow across the valve. This could be done either measuring flow directly or measuring the main poppet position and then calculating flow based on position and pressure drop. An observer design will also be considered in section 6.5 as a means of estimating flow using pressure measurements.

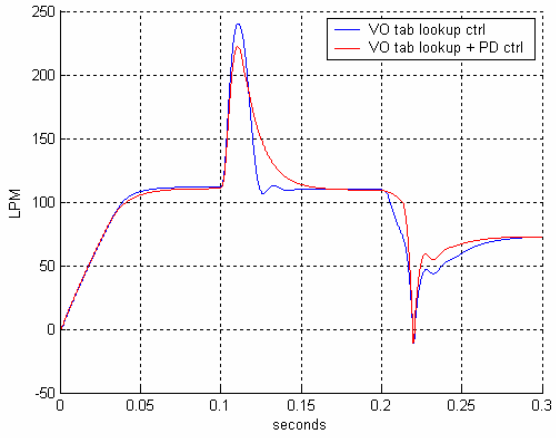

Fig. 6.10 Look-up table control vs. look-up plus PD control, desired flow 110 LPM, see Fig. 6.3 for pressure drop

Fig. 6.10 indicates that the addition of PD control reduces the spike in flow due to the sudden decrease in load pressure. Note that Fig. 6.10 and subsequent figures use table look-up control as shown in Fig. 6.4 as a benchmark for additional control designs. The constant orifice results are dropped from the figures because their inclusion only provides redundant information seen in previous figures. Fig. 6.11 and Fig. 6.12 display results for simulations where the load force is fixed while desired flow is varied at 0.1 and 0.3 seconds.

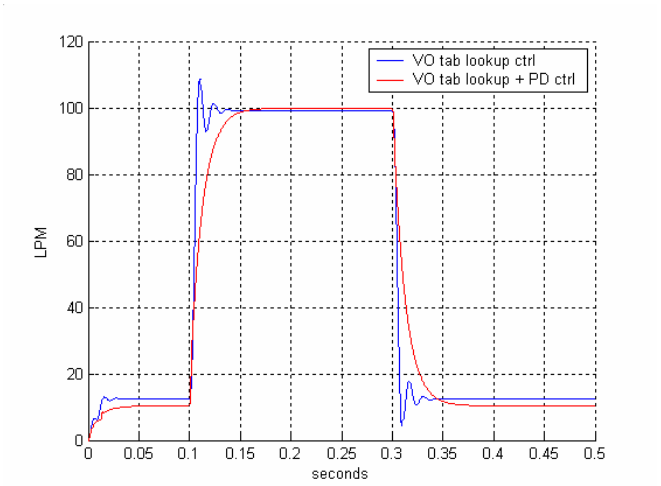

Fig. 6.11 Varying desired flow between 10 and 100 LPM, pressure drop approx 30MPa

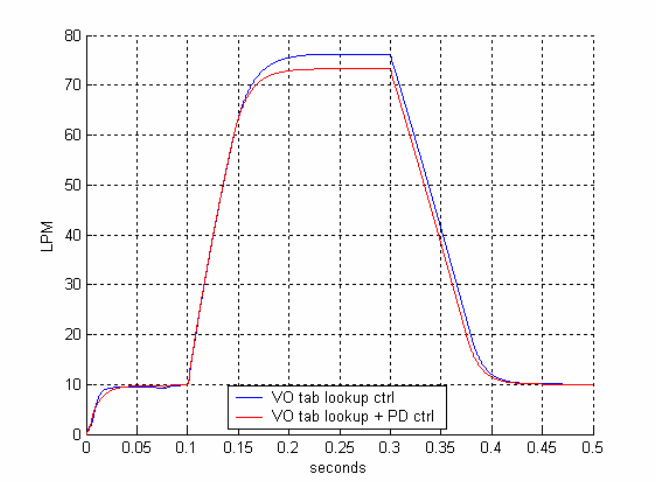

Fig. 6.12 Varying desired flow between 10 and 70 LPM, pressure drop approx 1 MPa

Results indicate that combining the look-up table with PD control reduces steady state error and provides damping to the transient response but does not reduce settling time.

6.3.3 Gain Scheduled PD Control:

The gains for the constant PD control shown in Fig. 6.9 were chosen by trial and error, but examining the root locus plots for the closed loop system with negative feedback suggests that the system could benefit from gain scheduling. Root locus plots are generated using the A and B matrices from Eq. ((5-8) while the C and D matrices come from Eq. (6-4), where the output is flow.

$$Y = \begin{bmatrix} kq_3 & 0 & kq_2 & 0 & kc_2 & 0 & (-kc_2 - kc_3) & 0 \end{bmatrix} \vec{X} + 0u \qquad (6\text{-}4)$$

Fig. 6.13 indicates that for high pressure drops the controller gain should be kept as small as possible to minimize overshoot and oscillation. Fig. 6.14 demonstrates that for low pressure drops increasing the controller gain can increase the system bandwidth without significantly jeopardizing overshoot or oscillation. In particular it is noted that the system would benefit from a control gain of 2×10^4 at 1 MPa pressure drop while the same gain would cause the system to be unstable at a 35 MPa pressure drop.

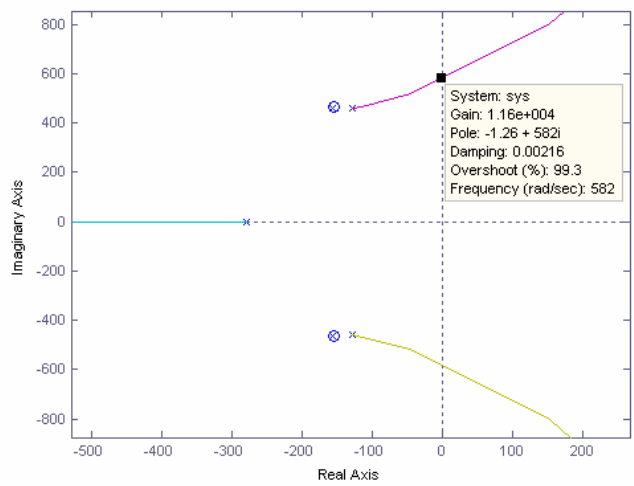

Fig. 6.13 Root locus for negative feedback of flow (35 MPa pressure drop)

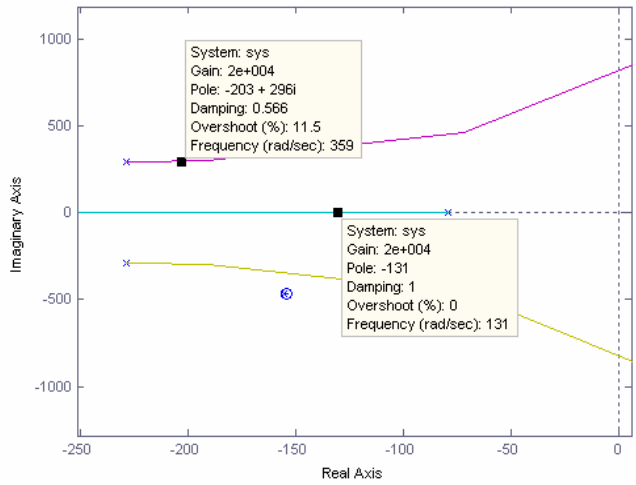

Fig. 6.14 Root locus for negative feedback of flow (1 MPa pressure drop)

Knowledge gained from root locus plots lead to the control design shown in Fig. 6.15. This control scheme creates a flow error signal in LPM and then converts it to meters cubed per second before entering the PD controller. As the pressure drop increases the proportional and derivative gains are decreased. The gain scheduling is contained in a simple linear look-up table and was tuned by trial and error to adjust damping and achieve acceptable steady-state error.

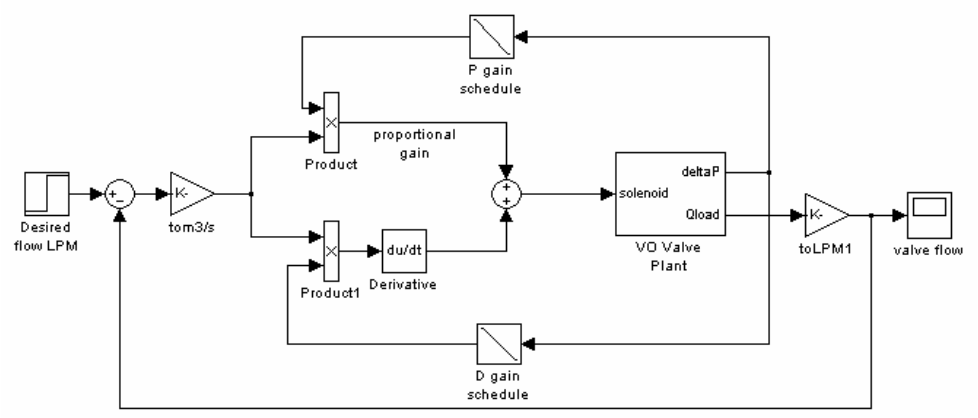

Fig. 6.15 Gain scheduled PD controller based on measured pressure drop

Fig. 6.16 shows that gain-scheduled PD control results in a smaller spike in flow as load pressure drops, as compared to look-up table control.

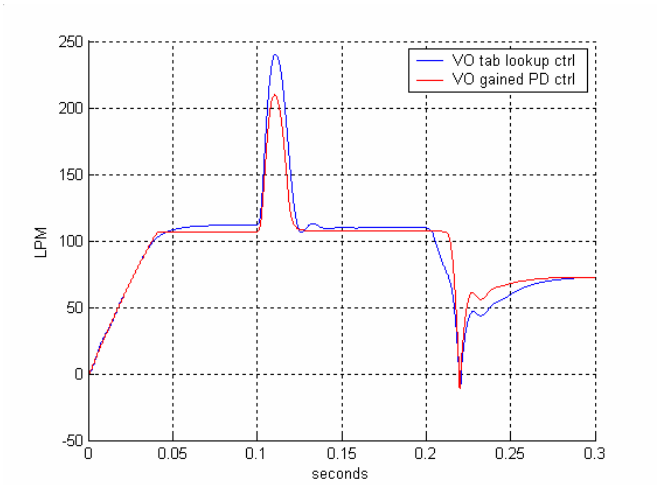

Fig. 6.16 Look-up table control vs. gain scheduled PD control, desired flow 110 LPM, see Fig. 6.3 for pressure drop

Fig. 6.17 shows that gain-scheduled PD control can be used to reduce oscillation at high pressure drops but Fig. 6.17 and Fig. 6.18 also emphasize that this control method is not the best for minimizing steady-state error.

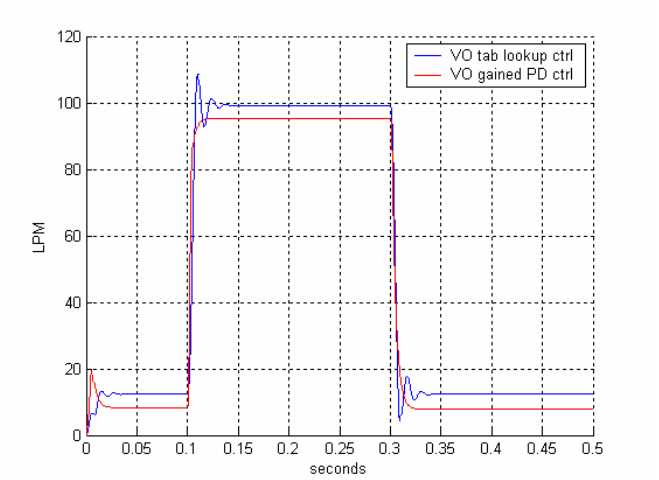

Fig. 6.17 Varying desired flow between 10 and 100 LPM, pressure drop approx 30 MPa

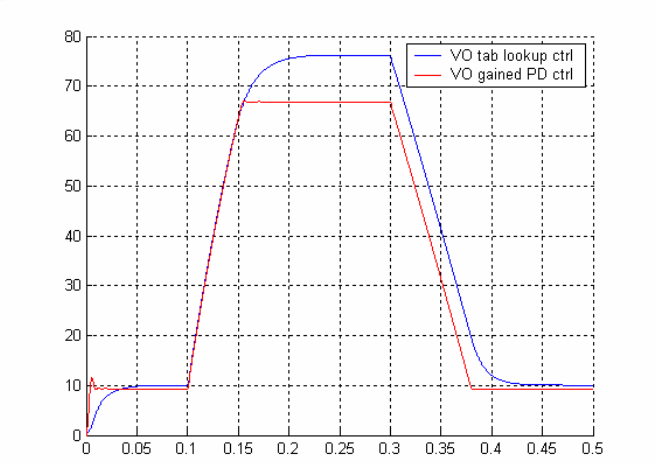

Fig. 6.18 Varying desired flow between 10 and 70 LPM, pressure drop approx 1 MPa

6.3.4 Table Look-up with Gain Scheduled PD Control:

The final controller that is examined employs both a look-up table and gain-scheduled PD control. The block diagram for this controller is shown in Fig. 6.19. Again, the gains for the PD control decrease as the pressure drop decreases but when the table look-up is included the gains are reduced so that the PD control effort is much smaller.

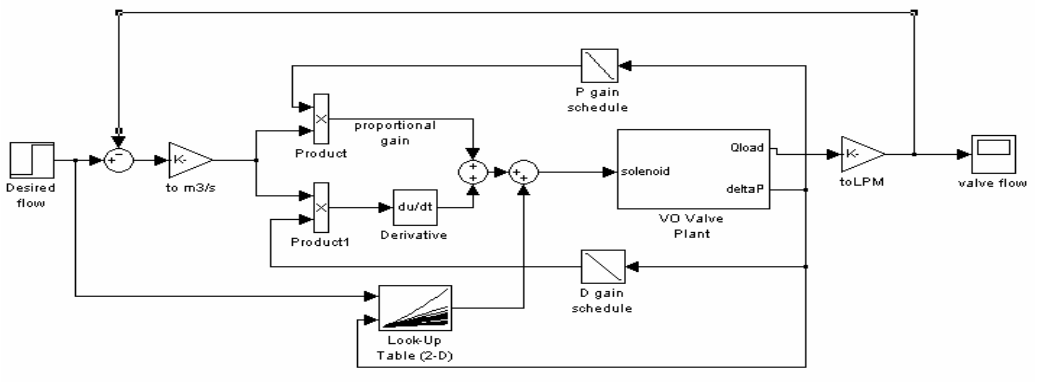

Fig. 6.19 Gain scheduled PD control with look-up table

Fig. 6.20 displays the response to changes in load pressure when desired flow is set to 110 LPM. Fig. 6.21 simulates changing the desired flow when the pressure drop is high, while Fig. 6.22 presents a similar simulation for the case of a low pressure drop. The effort with gain-scheduled PD control results in smaller transient spikes and less oscillation, as expected. In comparison with Fig. 6.17 and Fig. 6.18, gain scheduling the PD control effort provides a reduction in steady-state error.

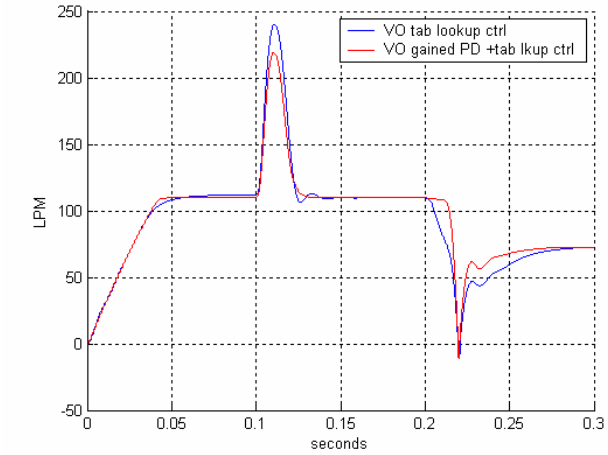

Fig. 6.20 Look-up table control vs. look-up table with gained PD control, desired flow 110 LPM, see Fig. 6.3 for pressure drop

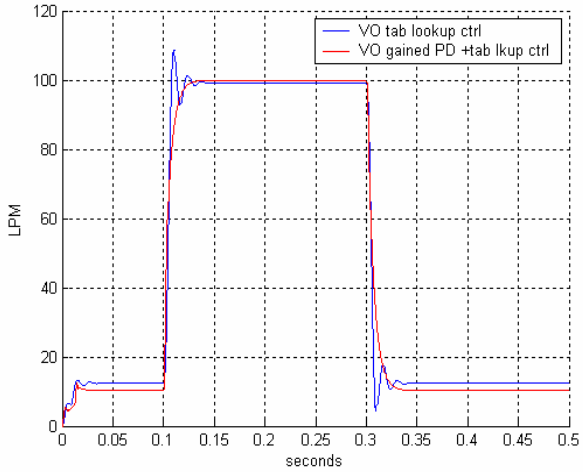

Fig. 6.21 Varying desired flow between 10 and 100 LPM, pressure drop approx 30MPa

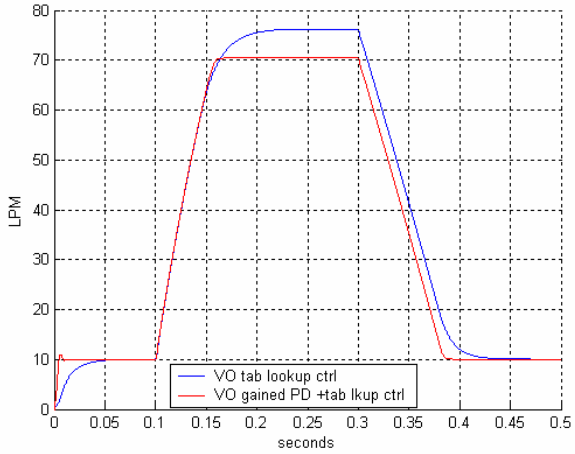

Fig. 6.22 Varying desired flow between 10 and 70 LPM, pressure drop approx 1 MPa

6.4 Flow Control Summary:

In efforts to maintain flow across the metering poppet valve, mechanical pressure compensation and four electronic controllers are presented and compared. A mechanical pressure compensator is best able to manage flow in response to extreme drops in the load pressure while it is the worst at minimizing steady-state error. The simplest electronic controller uses feedback of pressure

drop and a look-up table to drive the valve to the desired steady-state flow. The look-up table results in differing steady-state error as operating conditions vary but much of this error can be eliminated by refining the look-up table to include a larger array of pressure drops. At high pressure drops, the look-up table approach allows oscillation to occur but the system still responds quickly. The three remaining electronic controllers incorporated PD efforts on a flow error signal. The first, which combined constant PD control with the look-up table, was able to reduce transient spikes, provide damping, and reduce steady-state error. The second, which removed the look-up table and gain scheduled PD efforts based on pressure drop, was able to reduce transient spikes and provide damping but resulted in higher steady-state error. The last, which combined gain scheduled PD efforts with a look-up table, was able to reduce transient spikes and provide damping while leading to the lowest steady-state error.

6.5 Observer Design:

The majority of electronic controllers presented in this research employ feedback of valve flow. To avoid the cost of additional sensors it is advantageous to use the valve model to provide real time state estimates which can be used to calculate a flow estimate. Steps are taken here to create an observer which is limited to constant load force conditions. If results are positive, the methods undertaken will be useful in expanding the observer to function under all operating conditions.

The basic principle of an observer is that a model of the system should be

able to predict the transient states of the valve. The observer does not have knowledge of the real time initial conditions of the valve and so it makes use of real time measurements to synchronize itself with the system. In simple terms, the real system control effort is input to the valve model which mathematically responds and predicts the states. Lack of initial conditions means the model will be in error but real time measurements provide the observer knowledge of its error so that it can correct itself. In the case of the metering poppet valve, the error signal between estimated load pressure and measured load pressure is multiplied by a gain to synchronize model estimates with real time states.

Observer design typically makes use of a state-space model of the system. In this case the A and B matrices come from Eq. (5-8) while the measurement or output matrix, $C = \begin{bmatrix} 0 & 0 & 0 & 0 & 0 & 0 & 1 & 0 \end{bmatrix}$, and D = 0. The observer provides estimates of the 'true' states based on Eq. (6-5)

$$\dot{\hat{X}} = (A - K_e C)\hat{X} + \begin{bmatrix} B & \vdots & K_e \end{bmatrix} \begin{bmatrix} u \\ Y \end{bmatrix} \tag{6-5}$$

$$Y = load\ \ pressure\ measurement \qquad K_e = error\ gain\ matrix \qquad \hat{X} = state\ estimates$$

Existing computer algorithms can typically calculate the matrix K_e, given *A, C* and the desired estimator poles for the system [17]. Two difficulties are realized in this process. First, the system poles are not easily moved to any location but must be moved far enough to the left in the complex plane to ensure that the observer dynamics decay several times faster than the plant dynamics. A

feasible set of closed loop poles is found by considering the eigenvalues of the original A matrix and multiplying the real part by a factor of 8 and the imaginary part by a factor of 0.3. The second numerical difficulty arises due to a poorly scaled state-space system. In order to calculate the estimator gain matrix, K_e, it is necessary to perform a matrix transformation on the system such that $\vec{\bar{X}}_{transform} = T\vec{\bar{X}}$. The transformation allows for numerical calculation of $K_{e,transform}$ which can then be converted to K_e by calculating $T^{-1}K_{e,transform}$.

Once observer gains are calculated, simulations can be run to verify that the state estimates are able to quickly track the 'true' states. Performance requirements indicate that commanded valve flow must have a settling time of 0.1 seconds or less. This requirement indicates that an observer must be able to track actual flow in a small fraction of the demanded settling time. The comparison of observer estimates verses the 'true' states are shown in Fig. 6.23 through Fig. 6.30.

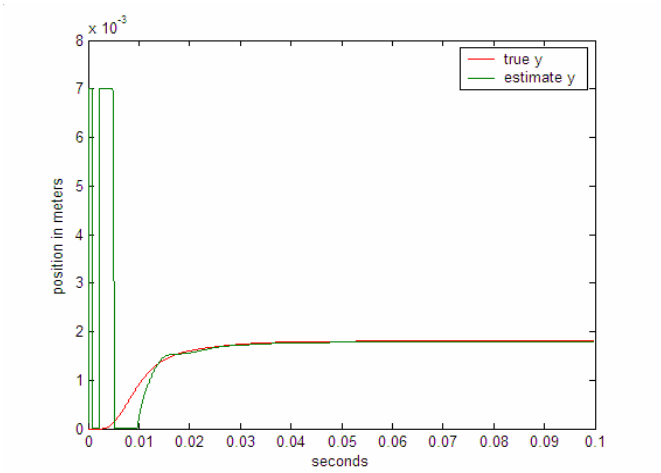

Fig. 6.23 Observer estimate of main poppet position

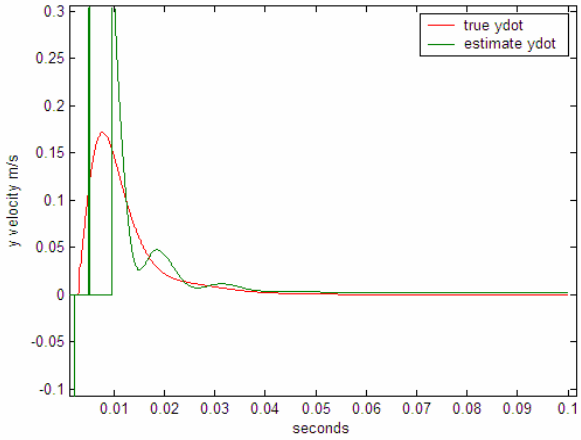

Fig. 6.24 Observer estimate of main poppet velocity

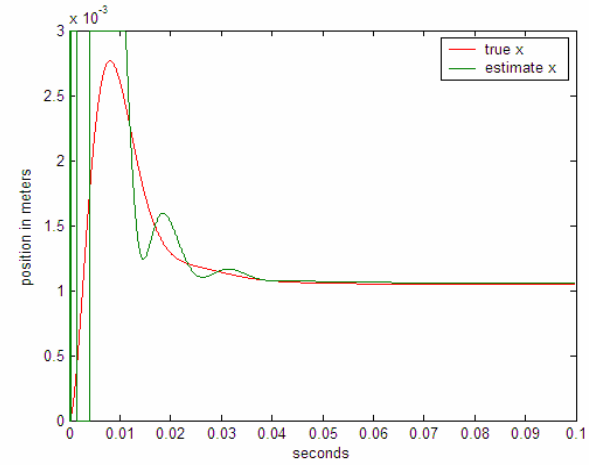

Fig. 6.25 Observer estimate of pilot poppet position

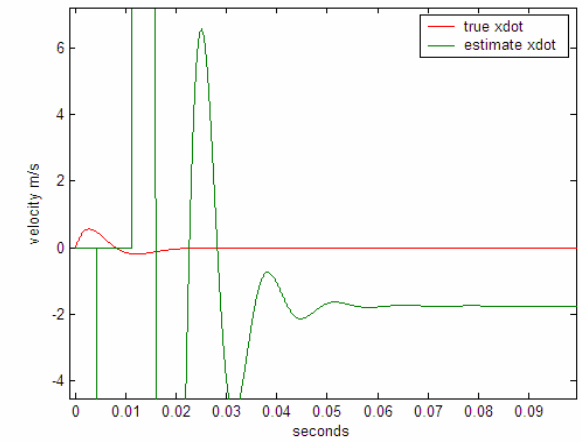

Fig. 6.26 Observer estimate of pilot poppet velocity

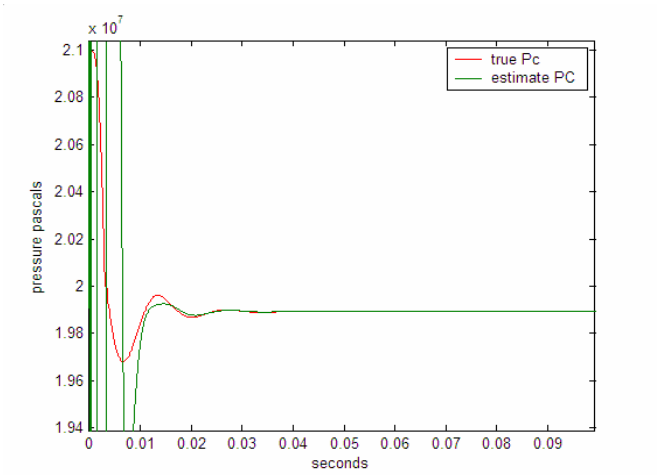

Fig. 6.27 Observer estimate of pressure above main poppet

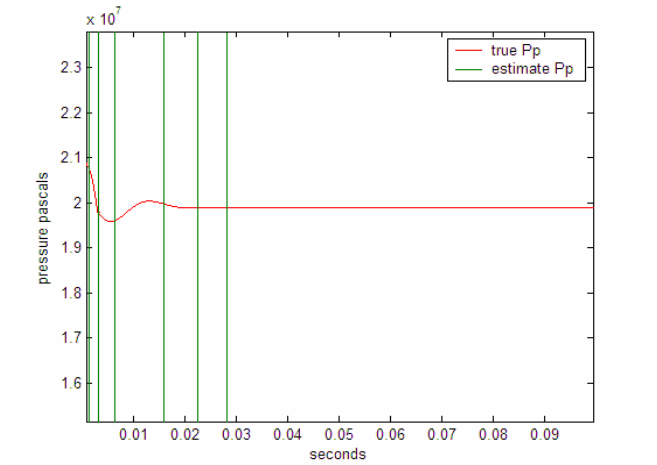

Fig. 6.28 Observer estimate of pressure above pilot poppet

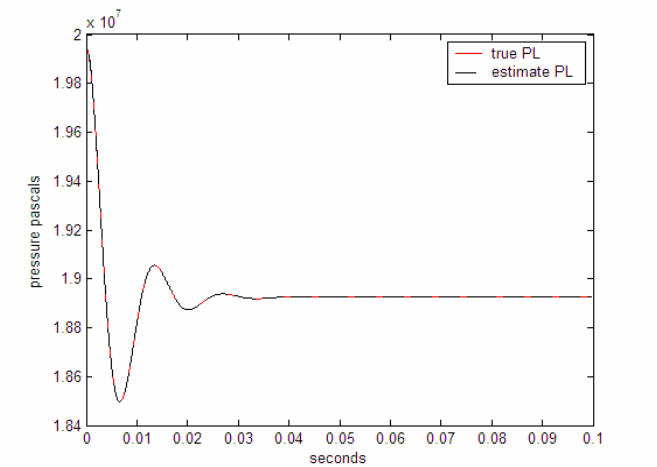

Fig. 6.29 Observer estimate of load pressure (measured)

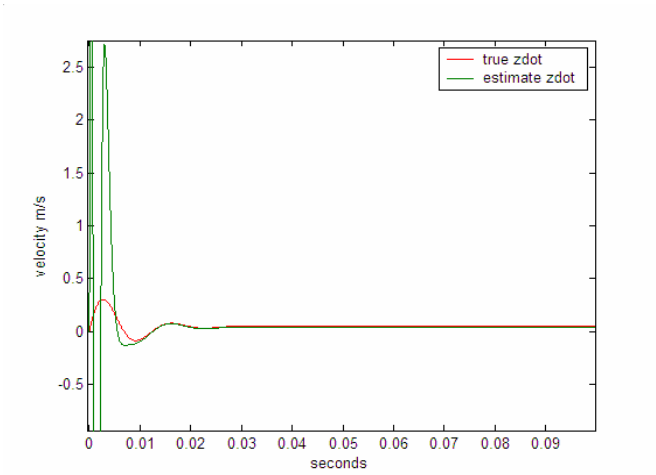

Fig. 6.30 Observer estimate of load piston velocity

Fig. 6.23 through Fig. 6.30 show that the observer tracks the 'true' states in less than 0.02 seconds for all cases except P_P and $\dot{x}$. Although faster tracking is desired, it is thought that 0.02 seconds will be adequate to provide desired performance. Past work comparing linear and nonlinear models indicates that better tracking should be obtained for P_P and $\dot{x}$ but it is thought this problem may arise due to the pole associated with P_P originally falling near -326,000 rad/s. Although tracking for P_P and $\dot{x}$ is not achieved this does not interfere with the ultimate goal of estimating flow. Equation (6-4) demonstrates that flow is not dependent on either P_P or $\dot{x}$ and therefore the observer designed will be adequate. Fig. 6.31 displays 'true' flow against the estimate of flow calculated from observer state estimates. These results suggest that a simpler model could be used for observer design in which the pilot poppet can be represented mathematically as was done in the 5-state model.

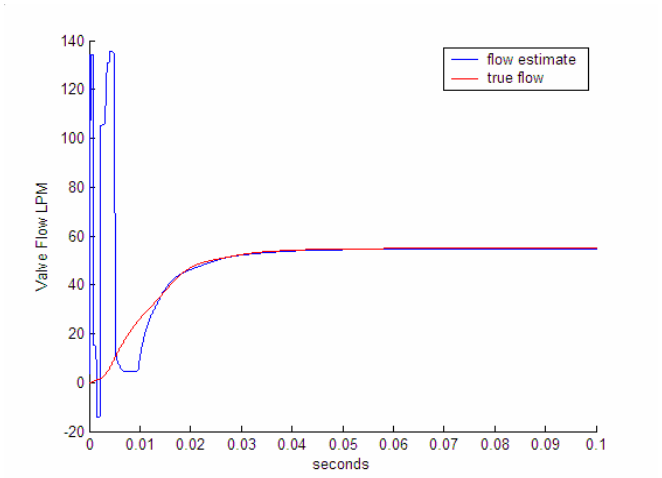

Fig. 6.31 Observer flow estimate vs. ‘true’ flow

CHAPTER 7

ROBUST CONTROL ANALYSIS

7.1 Introduction to Robust Analysis:

All control designs presented in this work are dependent on the accuracies of the valve models used. A true test of any control scheme requires implementing the controller on actual hardware. Although no hardware is available, an appropriate first step is to provide a robust control analysis. A robust control analysis will seek to determine if the system will remain stable and meet performance criteria even when the valve model is in error. This is done by examining the valve model and establishing which parameters and dynamics are most likely to be in error. Establishing error bands for parameters in the system provides a means to model uncertainty. Once an uncertainty model is calculated, it is possible to test for stability and performance under worst case conditions.

In particular, a robust control analysis is provided for the controller pictured in Fig. 6.9. Analysis of system performance will include examining nominal performance, NP, robust stability, RS, and robust performance, RP, as presented by Skogestad [18]. NP, RS, and RP criteria as presented here after are

dependent on the assumption that the valve control system is nominally stable. Although nominal stability has not been proven, this assumption is consistent with all modeling results that have been observed thus far.

7.2 Nominal Performance and the Sensitivity Transfer Function:

If a system is nominally stable it is then a logical next step to prove that NP is achieved. The sensitivity function, "S", the transfer function between the error signal and the reference input, is a good indicator of the closed-loop system performance. An upper bound transfer function, $1/|W_P(s)|$ can be placed on the magnitude of "S" to verify that a given set of performance criteria is met. $W_p(s)$ is a performance weighting function given by Eq. (7-1) where lower case "s" is the Laplace variable, "M" is maximum high-frequency error set equal to 2, "ω_b" is the desired system bandwidth set equal to 50.24 rad/s, and "A" is the maximum steady-state error set equal to 0.1.

$$W_p(s) = \frac{s/M + \omega_b}{s + \omega_b A} \tag{7-1}$$

Mathematically stated, |S| will meet performance requirements if the inequality in Eq. (7-2) is satisfied.

$$NP \Leftrightarrow |W_p(s)\mathrm{S}| < 1 \qquad \forall\ \omega \tag{7-2}$$

In order to present results for Eq. (7-2), the sensitivity transfer function must be determined from Fig. 6.9. To simplify the calculation of S, the pressure drop will

be assumed constant and therefore its feedback connected to the look-up table can be removed. This leaves negative flow feedback and a feedforward path which is only a function of the reference input. The simplified block diagram is shown in Fig. 7.1.

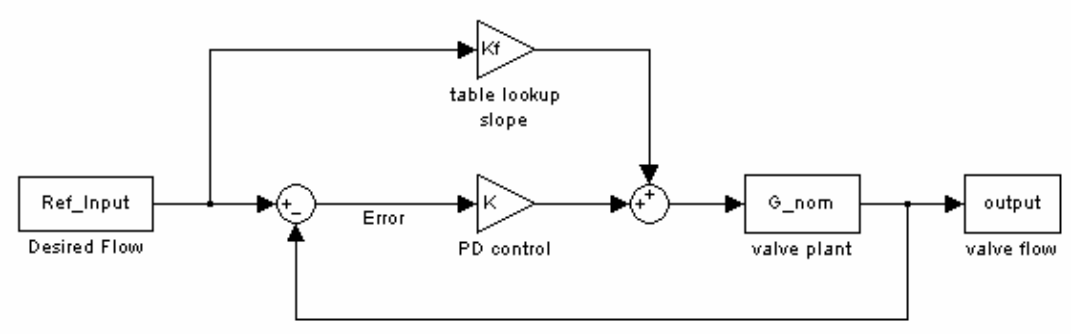

Fig. 7.1 PD/table look-up control with pressure drop held constant

Linear superposition makes it possible to break the two reference input paths of Fig. 7.1 into the two separate block diagrams shown in Fig. 7.2.

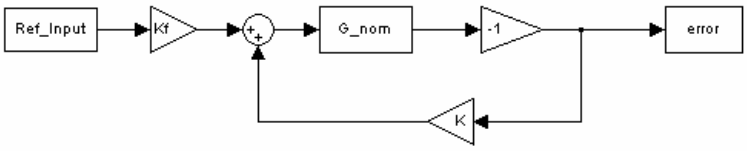

$$S_1 = \frac{E(s)}{R(s)} = \frac{1}{1+KG_{nom}}$$

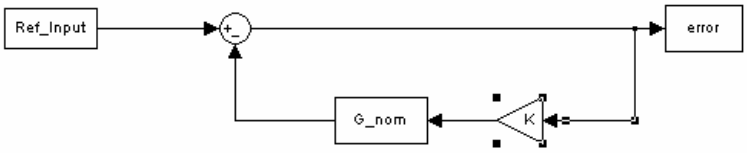

$$S_2 = \frac{E(s)}{R(s)} = \frac{-K_f G_{nom}}{1+KG_{nom}}$$

Fig. 7.2 Block diagram reduction for calculating sensitivity transfer function

S_1 plus S_2 from Fig. 7.2 gives the final system sensitivity shown in Eq. (7-3)

$$S = \frac{1 - K_f G_{nom}}{1 + G_{nom} K} \tag{7-3}$$

Here, K represents the transfer function for the PD control effort, K_f is a constant pressure slope from the look-up table, and G_{nom} is the transfer function for the linearized valve system. Because the above derivation of "S" assumes the pressure drop is constant, effects of pressure variation must be accounted for by analyzing an array of controllers. "S" is calculated for three different nominal plants with pressure drops of 1 MPa, 2.1 MPa, and 35 MPa. Fig. 7.3 plots on a logarithmic scale for all three pressure drops. Because $|W_P S|$ is less than 1 for all operating frequencies nominal performance is achieved for the tested pressure drops.

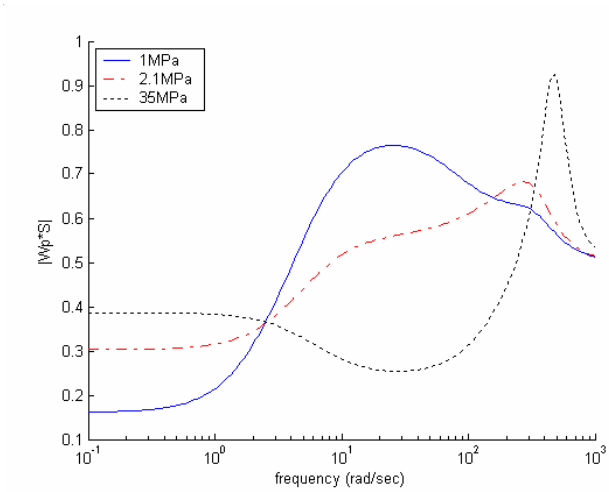

Fig. 7.3 Nominal Performance for 3 pressure drops when the valve is cracked open

7.3 Derivation of Robust Stability with Multiplicative Uncertainty:

To analyze robust stability, possible errors in the valve model must be considered as was discussed in section 7.1. This error will be considered by building multiplicative uncertainty into the model as is shown in Fig. 7.4.

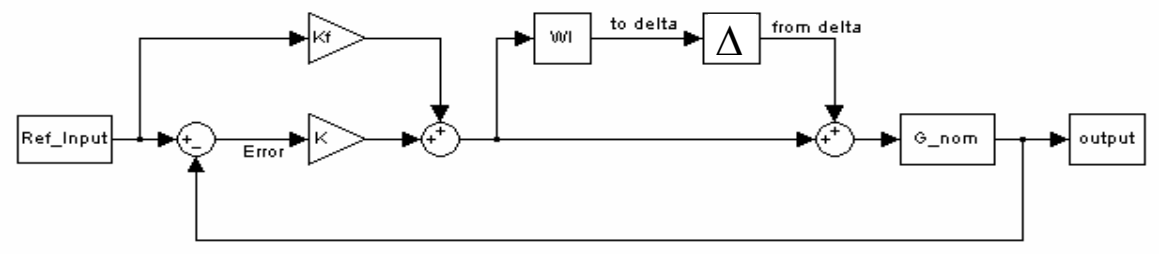

Fig. 7.4 Control scheme with multiplicative uncertainty included

The symbol Δ is the set of stable transfer functions whose magnitude is less than or equal to one, while W_I is the transfer function for the upper bound on uncertainty and is given by Eq.(7-4). Here G_p is the perturbed valve plant due to variation in system parameters (See sect 7.4 for calculation of G_p).

$$W_I(s) \geq \frac{\left|G_p(s) - G_{nom}(s)\right|}{\left|G_{nom}(s)\right|} \tag{7-4}$$

After multiplicative uncertainty is included in the system, Fig. 7.4 can be redrawn as Fig. 7.5 through basic block diagram reduction.

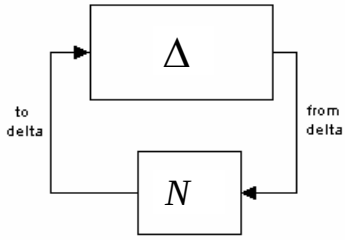

Fig. 7.5 $N\Delta$ configuration for determining RS criteria

Assuming nominal stability and applying the Nyquist stability condition to Fig. 7.5,

RS is achieved if and only if the loop transfer function $N\Delta$ does not encircle -1 for all Δ. Mathematically this criterion can be shown to reduce to Eq. (7-5).

$$RS \Leftrightarrow |N(s)| < 1 \qquad \forall \quad \omega \tag{7-5}$$

To find $N(s)$, the block diagram in Fig. 7.4 is reconfigured with "from delta" being the new system input and "to delta" being the new system output. The goal is to determine if there is instability due to W_I, therefore the flow output and the reference input paths can removed due to the NS requirement. The resulting block diagram manipulation is presented in Fig. 7.6 where the upper right most block represents $N(s)$.

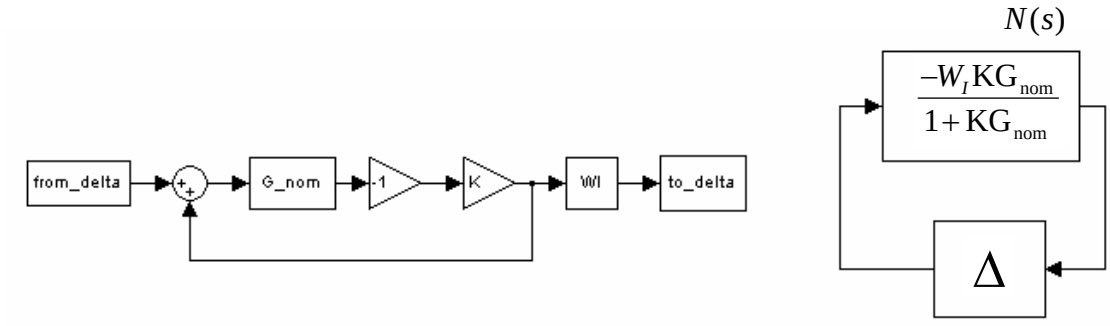

Fig. 7.6 Block diagram for determining robust stability criterion

Substituting the result of Fig. 7.6 into Eq. (7-5), the RS criterion now can be written as Eq. (7-6).

$$RS \Leftrightarrow \left| \frac{-W_I \mathrm{KG}_{\mathrm{nom}}}{1+\mathrm{KG}_{\mathrm{nom}}} \right| < 1 \qquad \forall \quad \omega \tag{7-6}$$

7.4 Multiplicative Uncertainty Weighting Function W_I:

The final step in the robust stability analysis is to establish W_I as given by

Eq. (7-4). This is done using a computer algorithm to calculate possible W_I as the plant is perturbed from the nominal model. Nested 'for' loops are used to vary uncertain plant parameters as they appear in the state matrix, Eq. (5-8). The following uncertainties are introduced as plant perturbations: $\beta \pm 30\%$, $k \pm 5\%$, $C_d \pm 10\%$, and $b_Z \pm 20\%$. In particular, the bulk modulus can vary due to entrained air or temperature changes, the spring constant is dependent on manufacturing tolerances, the orifice coefficient is known to vary with geometry and viscosity, and finally friction is always a parameter which is difficult to determine. Systematic variation of these uncertain parameters provides an array of possible W_I while the final transfer function must be an upper bound on all results found. Establishing W_I as the upper bound for all combinations of uncertainty ensures that the analysis is for the worst case plant. The final transfer function for weighting uncertainty is produced via an algorithm which fits a curve as well as a transfer function to the upper bound on all possible W_I. For each pressure drop examined it was possible to use a fourth order transfer function to fit W_I. Fig. 7.7 is a plot of possible multiplicative errors for a 1 MPa pressure drop while the red line represents the worst case W_I.

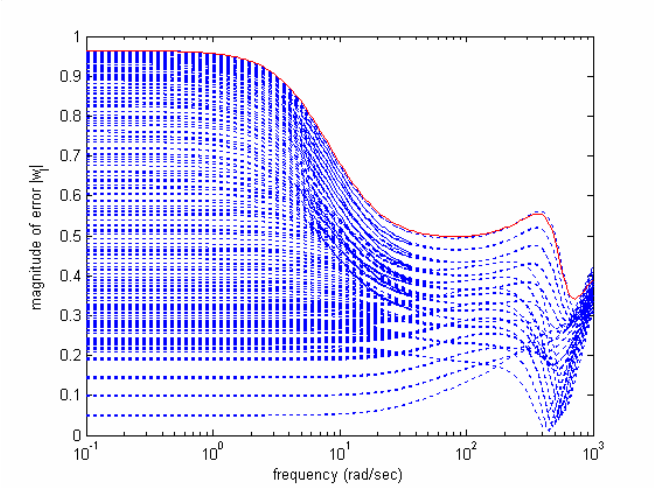

Fig. 7.7 W_I for worst case plant at 1 MPa pressure drop

7.5 Robust Stability and Performance Results:

Skogestad [18] shows that robust performance follows NP and RS as given in Eq. (7-7).

$$RP \Leftrightarrow \left|W_p S\right| + \left|N\right| < 1 \qquad \forall \qquad \omega \tag{7-7}$$

Once W_I has been calculated, plots of RS and RP easily follow and are shown in Fig. 7.8 and Fig. 7.9 Because the magnitude does not exceed one, these figures demonstrate that the valve control system of Fig. 6.9 achieves RS and RP for the uncertainty model and the nominal conditions considered.

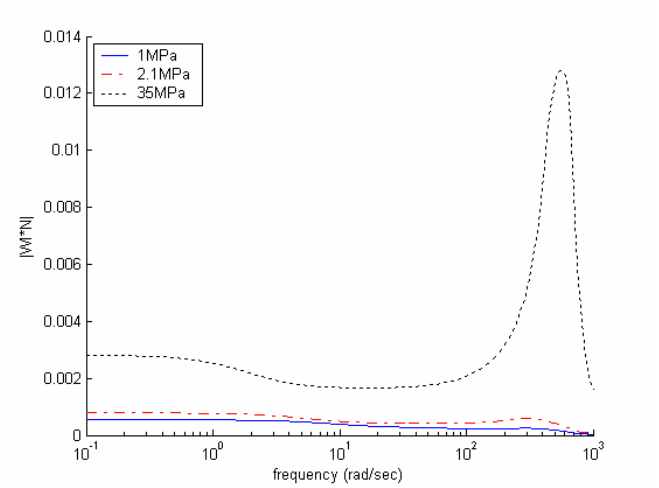

Fig. 7.8 Robust stability for 3 pressure drops with the valve cracked open

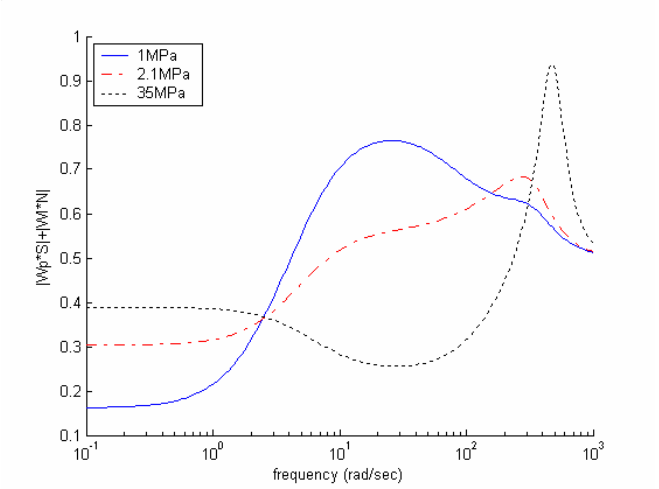

Fig. 7.9 Robust performance for 3 pressure drops with the valve cracked open

It must be emphasized that the robust analysis provided is only for one control scheme at three specific pressure drops. Although the analysis presented does not prove RP for the controller in question, it does provide a model which can be used to support RP. Future work must further examine the validity of the uncertainty model and expand the analysis to include a larger array of valve operation conditions.

CHAPTER 8

CONCLUSIONS

8.1 Overview:

In this thesis, root locus techniques were coupled with nonlinear simulations and Bode plots in efforts to design a forced-feedback metering poppet valve that is open-loop stable while meeting performance requirements. Two versions of the valve were presented (See Fig. 1.1 and Fig. 1.2), one with a fixed inlet orifice to the control volume and another with a variable inlet to the control volume. Root locus techniques indicated that the following design parameters had a key impact on stability and performance (actual values for design parameters can be found in the appendix).

a. The spring constant. (See Fig. 3.5 and Fig. 3.7)
b. The size or slope of the inlet orifice to the control volume. (Fig. 3.2)
c. The slope of the outlet orifice to the control volume (See Fig. 3.4)
d. System stability is highly dependent on effective pilot poppet damping. (See Fig. 3.6)

e. Stability design must focus on high pressure drop operation, while performance design must focus on low pressure drop operation.

While both the variable and constant orifice models could be tuned to achieve bandwidth requirements, the constant orifice model forced a trade off between performance and stability. It was shown that as the constant orifice was increased in size, the bandwidth could be increased but oscillation increased for high pressure drops. On the other hand, as the orifice was decreased in size, oscillation reduced while performance was hindered by a slow closing of the main poppet for low pressure drops.

Once valve design and modeling efforts had been thoroughly explored, mechanical and electronic flow control were presented. Mechanical pressure compensation provided the fastest response to sudden drops in load pressure but allowed high steady-state error and proved slower than electronic control under high pressure drops. (See Fig. 6.5 and Fig. 6.7) Several electronic controllers were presented using feedback of the pressure drop or feedback of pressure drop and load flow. The simplest controller (See Fig. 6.4) used a look-up table with pressure drop feedback to drive the system while the most complicated design (See Fig. 6.19) included the look-up table, feedback of both pressure and flow, and a gain scheduled PD controller. While the complex design did minimize overshoot, oscillation, and steady-state error, it came at the expense of having knowledge of the load flow. Due to the high cost and difficulty

of measuring flow, an initial attempt was made to design a flow estimator. In particular, an observer was successfully designed to estimate flow for the condition of constant load pressure (See Fig. 6.31). Finally, a Robust analysis of one control design (See Fig. 6.9) was presented which indicated that the system achieves robust stability and performance for the operating conditions which were examined.

8.2 Research Limitations:

Despite extensive efforts to model the important dynamics of a forced-feedback poppet valve there is no proof that this has been done. Assumptions have been presented and defended but until prototypes are built and tested the models herein are not supported by empirical evidence. While the work done in this thesis provides many insights into how various parameters impact a forced-feedback system, it does not provide a mathematical method for optimizing stability or performance. This limitation arises from the fact that the system is a highly nonlinear function of pressure. Although various nonlinear simulations were examined and linear techniques were applied to an array of pressure drops and valve openings, this method provides no guarantees.

8.3 Scope for Future Work:

Future work begins with prototyping the valve designs suggested and presenting empirical results. The results from both a constant orifice and variable orifice valve can be compared and contrasted with a manufacturing cost analysis for each design. With data available, the models presented can be

reduced to forms which include only the important dynamics. Mechanical and electronic control designs can be reexamined with the validated models and then tested with actual hardware. An observer design can also be implemented with reduced models and tested against actual measurements. Robust analysis can be expanded to more than one control scheme and a wider array of operating conditions.

APPENDIX

Parameter	*Description*	*Value*
Symbol $_O$	Any symbol followed by O subscript represents a nominal condition	
A_C	Area of main poppet exposed to control pressure	3.8e-4 m^2
A_{comp}	Area of ends of compensator spool	4.9e-4 m^2
A_L	Area of main poppet exposed to load pressure	1.9e-4 m^2
A_S	Area of main poppet exposed to supply pressure	1.9e-4 m^2
A_{pilot}	Area of pilot poppet exposed to pilot pressure	5e-5 m^2
A_{pist}	Area of load piston exposed to load pressure	1.1209e-2 m^2
a_1	Area of inlet orifice to control volume (variable orifice)	(-3.208e-4 x +1.1375e-6) m^2
a_{1fix}	Area of inlet orifice to control volume (constant orifice)	4.375e-7 m^2
a_{1max}	Area of variable inlet orifice when poppet is closed	1.1375e-6 m^2
a_2	Area of outlet orifice to control volume	8.16e-4 x
a_3	Area of the main poppet orifice	6.38e-3 y
a_{4fix}	Area of orifice from load volume to tank (establishes desired ΔP)	m^2
a_{comp}	Area of compensator orifice (varies nonlinearly with x_{comp})	(1e-2 to 7e-6) m^2
B_X	Artificial pilot poppet damping (lumping linear plus nonlinear)	15.75 N-s/m
b_{comp}	Damping of compensator spool	500 N-s/m
b_X	Linear pilot poppet damping	1.4 N-s/m
b_Y	Main poppet damping	1.8 N-s/m
b_Z	Load piston damping	17000 N-s/m
C_d	Orifice discharge coefficient	.62
$F_{c.pre}$	Spring preload on compensator spool	981.7 N
F_{load}	Working load force on the load piston	211,400 N
F	Actuator input force to the pilot poppet	(0-60) N
h_1	Slope to control volume inlet orifice (for variable orifice model)	-3.208e-4 m

h_2	Slope to control volume outlet orifice	8.16e-4 m
h_3	Slope to the main poppet orifice	6.38e-3 m
k	Feedback spring coefficient	7000 N/m
k_{comp}	Compensator spring coefficient	10,000 N/m
$kc_{(1-4)}$	Pressure flow coefficient for orifices 1 – 4	Function of nominal
kcp	Pressure flow coefficient for the pilot tube	1.2272e-10
$kfc_{(1-3)}$	Pressure flow force coefficient for orifices 1 – 3	Function of nominal
$kfq_{(1-3)}$	Flow force gain for orifices 1 – 3	Function of nominal
$kq_{(1-3)}$	Flow gain for orifices 1 – 3	Function of nominal
L_{pilot}	Pilot tube length	0.02 m
M	Mass of the main poppet	0.166 kg
M_{pist}	Mass of the load piston	55 kg
m	Mass of the pilot poppet	0.0415 kg
m_{comp}	Mass of compensator spool	0.06 kg
P_C	Control volume pressure	Pa
$P_{s,c}$	Pressure between compensator and poppet valve	Pa
P_L	Fluid pressure between the valve and the load piston	Pa
P_p	Pressure between the pilot poppet and the actuator housing	Pa
P_S	Fixed supply pressure	21 MPa
P_T	Fixed tank pressure	101,000 Pa
preload	Initial displacement of feedback spring	5e-6 m
Q_1	Flow rate across inlet orifice to control volume	m^3/s
Q_2	Flow rate across outlet orifice from control volume	m^3/s
Q_3	Flow rate across main poppet orifice	m^3/s
Q_4	Flow rate across load orifice	m^3/s
Q_6	Flow rate through the pilot poppet tube	m^3/s
Q_{comp}	Flow rate across pressure compensator orifice	m^3/s
R	Radius of pilot tube	0.0005 m
V_C	Fluid volume between main poppet and pilot poppet when closed	8.36e-6 m^3

V_L	Fluid volume between valve and load orifice	0.002 m^3
V_{Load}	Fluid volume between the valve and the retracted load piston	1.27895e-2 m^3
V_P	Fluid volume between closed pilot poppet and solenoid housing	5e-7 m^3
x	Position of the pilot poppet (positive is down in Fig. 1)	(0-3) mm
x_{comp}	Position of the compensator spool	(0-3) mm
x_n	Pilot poppet position referenced from the nominal opening	m
y	Position of the main poppet (positive is up in Fig. 1)	(0-7)mm
y_n	Main poppet position referenced from the nominal opening	m
z	Position of the load piston	m/s
β	Fluid bulk modulus	1.334e9 Pa
ρ	Fluid density	833 kg/m^3
μ	Fluid viscosity	0.01 $N\text{-}s/m^2$

REFERENCES

[1] Zhang, R., Alleyne, A. G., Prasetiawan, E. A., “Performance Limitations of a Class of Two-Stage Electro-Hydraulic Flow Valves,” International Journal of Fluid Power, Vol. 3, 2002, No. (1).

[2] Schexnayder, L. F., , “Poppet Valve with Force Feedback Control,” U.S. Patent 5 421 545, Jun. 6, 1995.

[3] Aardema, J. A., 1997, “Pilot Valve for a Flow Amplyifying Poppet Valve,” U.S. Patent 5 645 263, Jul. 8, 1997.

[4] Yang, X., Paik, M. J., Pfaff, J. L., “Pilot Operated Control Valve Having a Poppet With Integral Pressure Compensating Mechanism,” U.S. Patent 6 745 992, Jun. 8, 2004.

[5] Yang, X., Stephenson, D. B., Paik, M. J., “Hydraulic Poppet Valve with Force Feedback,” U.S. Patent 6 869 060, Mar. 22, 2005.

[6] Manring, N. D., *Hydraulic Control Systems*, Hoboken, NJ: John Wiley & Sons, 2005, pp. 224-228

[7] Merritt, H. E., *Hydraulic Control Systems*, New York: John Wiley & Sons, 1967.

[8] Hayashi, S., 1995, “Instability of Poppet Valve Circuit,” JSME International Journal Series C, Vol. 38, No. (3), pp. 357-366

[9] Funk, J. E., “Poppet Valve Stability,” Journal of Basic Engineering, June 1964, pp. 207-212

[10] Wandling, D. E., Johnson, B. L., 1972. “Hydraulic Poppet Valve Stability.” SAE National Combined Farm, Construction & Industrial Machinery and Powerplant Meetings, Milwaukee, WI.

[11] McCloy, D., “Compensation of Steady State Flow Forces in Valves,” Hydraulic Pneumatic Power, March 1969, pp. 150-158

[12] Johnston, D., K. Edge, N. Vaughan. 1991. “Experimental Investigation of Flow and Force Characteristics of Hydraulic Poppet and Disc Valves.” Proceedings of the Institution of Mechanical Engineers Part A, Vol. 205, No. (A3), pp. 161-171

[13] Fales, R. 2005. “Stability and Performance Analysis of a Metering Poppet Valve.” ASME International Mechanical Engineering Congress and Exposition, Orlando, FL.

[14] Opdenbosch, P., Sadegh, N., Book, W., 2004. “Modeling and Control of an Electo-hydraulic Poppet Valve.” ASME International Mechanical Engineering Congress and Exposition, Anaheim, CA.

[15] Li, P. Y., 2002, “Dynamic Redesign of a Flow Control Servovalve Using a Pressure Control Pilot,” Journal of Dynamic Systems, Measurement, and Control, Vol. 124, pp 428-434

[16] White, F. M., *Fluid Mechanics*, New York, NY: McGraw Hill, 2003.

[17] Ogata, K., *Modern Control Engineering*, Upper Saddle River, NJ: Prentice Hall, 2001.

[18] Skogestad, S., Postlethwaite, I., *Multivariable Feedback Control, Analysis and Design*, Chichester, England: John Wiley & Sons, 1996.